Annu. Rev. Astron. Astrophys. 2003. 41:117–67
doi: 10.1146/annurev.astro.41.082801.100328

First published online as a Review in Advance on June 4, 2003

MASS LOSS FROM THE NUCLEI OF ACTIVE GALAXIES

D. Michael Crenshaw
Department of Physics and Astronomy, Georgia State University, Atlanta, Georgia 30303; email: crenshaw@chara.gsu.edu

Steven B. Kraemer
The Catholic University of America and Laboratory for Astronomy and Solar Physics, NASA's Goddard Space Flight Center, Greenbelt, Maryland 20771; email: stiskraemer@yancey.gsfc.nasa.gov

Ian M. George
Joint Center for Astrophysics, University of Maryland, Baltimore County, Baltimore, Maryland 21250 and Laboratory for High Energy Astrophysics, NASA's Goddard Space Flight Center, Greenbelt, Maryland 20771; email: ian.george@umbc.edu

Key Words Seyfert galaxies, quasars, outflow, intrinsic absorption, warm absorber

■ **Abstract** Blueshifted absorption lines in the UV and X-ray spectra of active galaxies reveal the presence of massive outflows of ionized gas from their nuclei. The "intrinsic" UV and X-ray absorbers show large global covering factors of the central continuum source, and the inferred mass loss rates are comparable to the mass accretion rates. Many absorbers show variable ionic column densities, which are attributed to a combination of variable ionizing flux and motion of gas into and out of the line of sight. Detailed studies of the intrinsic absorbers, with the assistance of monitoring observations and photoionization models, provide constraints on their kinematics, physical conditions, and locations relative to the central continuum source, which range from the inner nucleus ($\sim$0.01 pc) to the galactic disk or halo ($\sim$10 kpc). Dynamical models that make use of thermal winds, radiation pressure, and/or hydromagnetic flows have reached a level of sophistication that permits comparisons with the observational constraints.

1. MASS OUTFLOW AND INTRINSIC ABSORPTION

The basic picture of an active galactic nucleus includes a supermassive black hole (SMBH) in the central gravitational well of the host galaxy, a surrounding accretion disk responsible for most of the continuum radiation from the infrared to "soft" ($\lesssim$1 keV) X-rays, a hot corona that produces "hard" ($\gtrsim$1 keV) X-rays near the SMBH, and rapidly moving clouds of ionized gas that produce emission lines. These components are found in the spectra of most classes of active galactic

nuclei (AGN) over a huge range in bolometric luminosity, from dwarf Seyfert galaxies to high-redshift quasars ($L_{bol} = 10^{40}$–10^{47} ergs s^{-1}). Additional components detected in subsets of AGN have also been known for decades; these are interesting in that they reveal mass outflow from the nucleus. "Radio-loud" AGN show collimated jets of relativistic plasma and/or associated lobes that are detected primarily by their radio synchrotron radiation; roughly 5%–10% of quasars are radio-loud (see Peterson 1997). In addition, ∼10% of radio-quiet quasars show broad absorption lines (BALs) in their rest-frame ultraviolet (UV) (912–3200 Å) with blueshifted velocities as large as ∼0.1 c with respect to the emission lines (Weymann et al. 1981). Given these percentages, one might wonder if mass loss is an important component in the overall structure of most AGN. However, recent UV and X-ray (∼0.3–12 keV; 1–40 Å) observations have detected outflowing clouds of ionized gas in a majority of the moderate luminosity Seyfert galaxies, emphasizing the importance of mass loss. The outflowing clouds are revealed through "intrinsic" absorption lines that are blueshifted with respect to the systemic (redshifted) velocity of the AGN. This article is a review of the intrinsic absorption phenomenon in AGN, with particular emphasis on Seyfert galaxies (Seyfert 1943). Recent results on other forms of mass loss (including evidence for outflow in the emission-line regions) can be found in Crenshaw et al. (2002a); these results are mentioned when appropriate.

1.1. Intrinsic UV and X-Ray Absorption

Here, the term Seyfert galaxy refers to AGN with moderate luminosities ($L_{bol} = 10^{43}$–10^{45} ergs s^{-1}) that are relatively nearby ($z < 0.1$). Seyfert galaxies are the brightest AGN in the sky and hence ideal candidates for studies of intrinsic absorption at moderate or high spectral resolution. The optical and UV spectra of Seyfert 1 galaxies show broad permitted emission lines [full width at half-maximum (FWHM) > 1000 km s^{-1}] and narrow permitted and forbidden emission lines (FWHM $\leq$ 500 km s^{-1}), whereas Seyfert 2 galaxies only show the narrow lines (Khachikian & Weedman 1971). The optical, UV, and X-ray spectra of Seyfert 1 galaxies are dominated by nonstellar continua that are typically characterized by power laws, whereas this emission is much weaker in Seyfert 2 galaxies. Within the current unification paradigm (see Antonucci 1993), the intrinsic nonstellar continua and broad emission lines are similar for both classes, but obscuring material along the line of sight greatly attenuates the emission from the inner nucleus in Seyfert 2 galaxies from the optical to medium (∼few keV) X-ray bands. Thus, studies of intrinsic absorption concentrate on Seyfert 1 galaxies and broad-lined quasars for the practical reason that it is much easier to detect the absorption against strong nuclear continua and/or broad emission lines.

Approximately 60% of Seyfert 1 galaxies show intrinsic UV absorption in the 1200–3200 Å band (Crenshaw et al. 1999). These lines can be detected at moderate spectral resolving power ($R \equiv \lambda/\Delta\lambda \approx 1000$, where λ is the observed wavelength and $\Delta\lambda$ is the FWHM of an unresolved line), as shown by the UV spectrum of the Seyfert 1 galaxy NGC 5548 in the top panel of Figure 1, which was obtained with

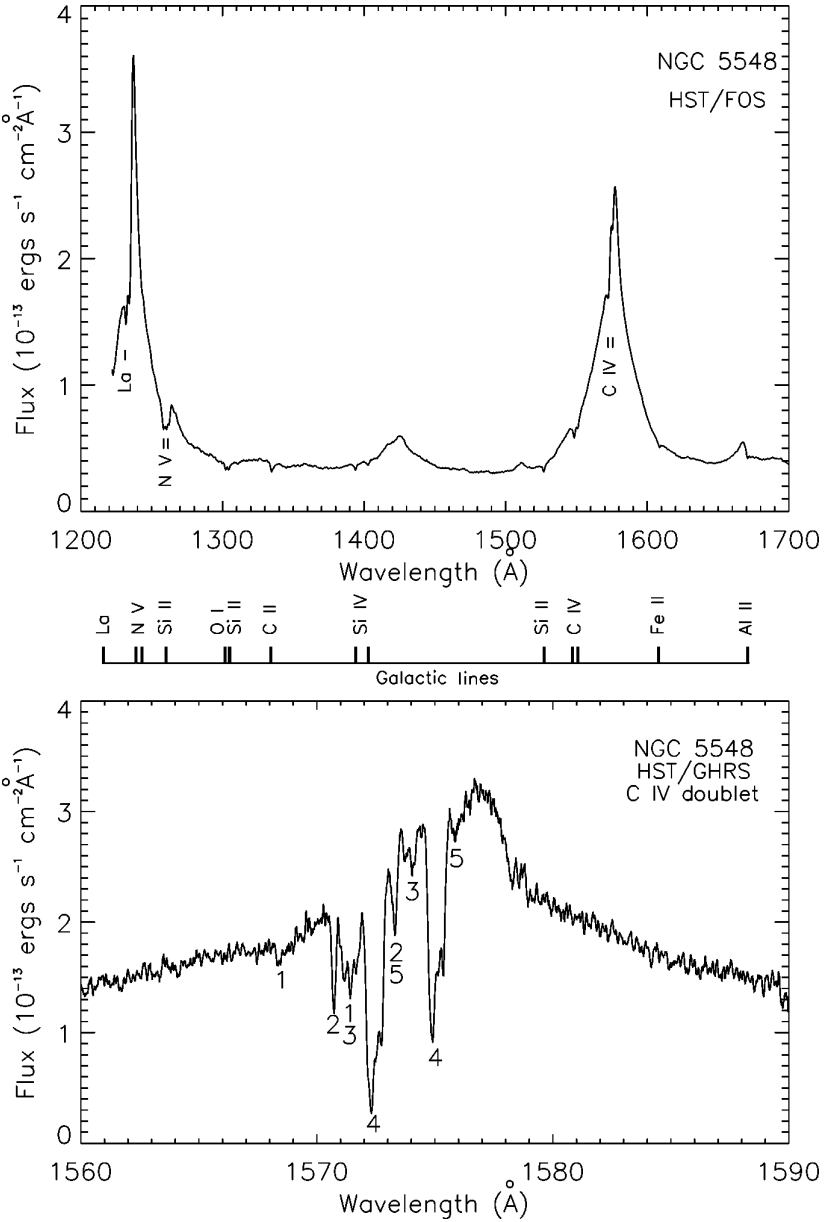

Figure 1 HST spectra of the Seyfert 1 galaxy NGC 5548. The top panel shows a spectrum from the FOS and indicates the positions of intrinsic UV absorption by H I Lα and the C IV and N V doublets. The middle panel shows the locations of interstellar absorption lines in the top panel due to our Galaxy. The bottom panel shows a high-resolution spectrum in the C IV region from the GHRS and identifies five kinematic components of absorption in the C IV doublet.

the Faint Object Spectrograph (FOS) (Harms & Fitch 1991) on the Hubble Space Telescope (HST). This is a typical UV spectrum of a Seyfert 1 galaxy in that it shows a strong nonstellar continuum, broad emission lines, narrow components to the emission lines, and absorption lines from the interstellar medium (ISM) of our Galaxy (identified in the middle panel of Figure 1). The intrinsic UV absorption lines seen in NGC 5548 are also typical. The most common of these are due to electric dipole transitions from the ground-state ($1s^2 2s\ ^2$S) of Li-like ions of C, N, and O to the $1s^2 2p\ ^2$P^0 state. Observations at high spectral resolution are required to fully characterize these absorption lines, as demonstrated by the HST spectrum of NGC 5548 in the bottom panel of Figure 1; this spectrum was obtained by the Goddard High-Resolution Spectrograph (GHRS) (Brandt et al. 1994) at $R = 20{,}000$ in the region around the broad C IV emission line. At this resolution, the doublet nature of the line (λλ 1548.2, 1550.8, corresponding to the $^2P^0_{3/2}$ and $^2P^0_{1/2}$ terms in the final state, respectively) is resolved, and it is clear that the intrinsic absorption actually consists of multiple kinematic components.

Regarding the ionic species detected via intrinsic UV absorption lines in Seyfert 1 galaxies, the C IV λλ 1548.2, 1550.8; N V λλ 1238.8, 1242.8; and O VI λλ 1031.9, 1037.6 doublets are always present in addition to the 1*s*–2*p* transition in H I Lyα λ1215.7 (Crenshaw et al. 1999, Kriss 2002). The ionization potentials (IPs) required to create C IV, N V, and O VI are 47.9, 77.5 m, and 113.9 eV, respectively, which indicates the gas is in a relatively high state of ionization (although there is still a sufficient column density of H I in the gas to produce a measurable Lyα absorption line). Absorption lines from ions with lower IPs occur less frequently: Si IV λλ1393.8, 1402.8 (IP = 34.8 eV) and Mg II λλ2796.3, 2803.5 (IP = 7.6 eV) are seen in ∼40% and ∼10% of Seyfert 1 galaxies with intrinsic absorption, respectively (Crenshaw et al. 1999).

A general characteristic of intrinsic UV absorption in Seyfert 1 galaxies is that almost all the kinematic components are blueshifted with respect to the systemic velocities of the host galaxies (see Figure 1). Thus, the absorbing gas is outflowing with radial velocities ranging from ∼zero to about −2100 km s^{-1} (Crenshaw et al. 1999). At a resoving power $R = 20{,}000$ (corresponding to a velocity resolution of 15 km s^{-1}), the absorption components are almost always resolved, with widths ranging from 20 to 400 km s^{-1} (FWHM). These widths are typically much broader than the expected thermal widths (e.g., FWHM ≈ 9 km s^{-1} for carbon at a temperature $T = 20{,}000$ K), indicating macroscopic motions within a component. In nearly all Seyfert 1 galaxies with absorption, the depth of at least one kinematic component is sufficiently large to indicate that the gas absorbs both the continuum and broad emission-line fluxes (e.g., component 4 in NGC 5548; Figure 1) and therefore it lies outside of the broad emission-line region (BELR).

Given column densities N_H ($= N_{HI} + N_{HII}$) of at least 10^{20} cm^{-2}, photoelectric absorption by the ISM in both our Galaxy and the AGN host galaxy makes the observation of extragalactic objects extremely difficult at energies between 13.6 eV (912 Å; the H I bound/free absorption edge) and ∼300 eV (∼40 Å). This prevents the study of absorption using the $1s^2 2s$–$1s^2 2p$ doublets of Li-like ions

with atomic number $Z > 8$ (e.g., Ne VIII λλ770.4, 780.3) in low-redshift AGN, as well as the higher-order lines in the $1s^2 2s$–$1s^2 np$ ($n = 3, 4, 5\ldots$) series of C IV, N V, and O VI. Thus, there are only a limited number of absorption lines in the UV to provide diagnostics of high-ionization gas, although many more lines are available for lower ionization gas (see Kraemer et al. 2001b).

X-ray photons are sufficiently energetic to excite or ionize inner-shell electrons of all the cosmically abundant elements from C to Ni [primarily *K*-shell electrons ($n = 1$)] and transitions from higher shells in the case of the high-*Z* elements such as Fe. As discussed further in Section 1.2.2, studies of the photoelectric bound/free absorption edges (most noteably those of O VII and O VIII) over the last decade have suggested a large fraction of Seyfert 1 galaxies show evidence for intrinsic absorption by highly ionized gas. However, the ability to determine the kinematics and detailed characteristics from X-ray spectroscopy has only been possible for the past few years following the launch of the Chandra X-Ray Observatory (CXO) (Weisskopf et al. 1996) and the XMM-Newton Space Observatory (Jansen et al. 2001). These missions provided grating spectrometers behind mirrors with sufficient collecting area to enable detailed spectroscopic studies with $R \gtrsim 100$ at 1 keV.

The first observations of Seyfert galaxies employing the CXO and XMM-Newton gratings have confirmed that indeed large quantities of highly ionized gas lie within the circumnuclear regions of a large fraction of Seyfert galaxies. Figure 2 shows two sections of the CXO grating spectrum of the Seyfert 1 galaxy NGC 3783 (adapted from Kaspi et al. 2002). The strong nonstellar continuum is imprinted with a large number of absorption lines. In the upper panel of Figure 2, the location of the first nine K-shell lines ($n = 1 \rightarrow 2, 3, \ldots 10$) for the He- and H-like ions Si XIII and Si XIV are indicated, along with the location of the corresponding bound/free edges. It can be seen that many of these lines are detected. In addition, a number of lines due to less-ionized Si are detected, along with several lines of Mg, Al, and S. The lower panel of Figure 2 illustrates the richness of the data now available and highlights the analysis challenge. Several He- and H-like lines of Ne are detected, but they are surrounded by a forest of Fe lines from a wide range of ionization states (see Kaspi et al. 2002 for the full CXO spectrum). In the observations of Seyfert 1 galaxies reported to date, the detected *K*-shell lines range in wavelength from C V λ40.268 ($1s^2 \rightarrow 1s2p$) to Ca XX λ2.5494 ($1s \rightarrow 3p$) with creation IPs in the range 64.5 eV to 5.13 keV.

From close inspection of Figure 2 it can be seen that the lines are blueshifted relative to the systemic velocity of NGC 3783. As in the UV, this is a common trait of intrinsic absorption lines observed in the X-ray band. The lines observed in several sources, including NGC 3783 (Kaspi et al. 2000, 2001, 2002), NGC 5548 (e.g., Kaastra et al. 2000, 2002), and NGC 4051 (Collinge et al. 2001), indicate the absorbing material is outflowing from the nucleus with radial velocities up to ~ -2400 km s^{-1}. In addition, there is clear evidence that in at least some sources many of the lines are broader than the instrumental resolution, with FWHM $\approx$ 800 km s^{-1}. The total column densities (summed over all kinematic components) implied by these early results are broadly consistent with the results

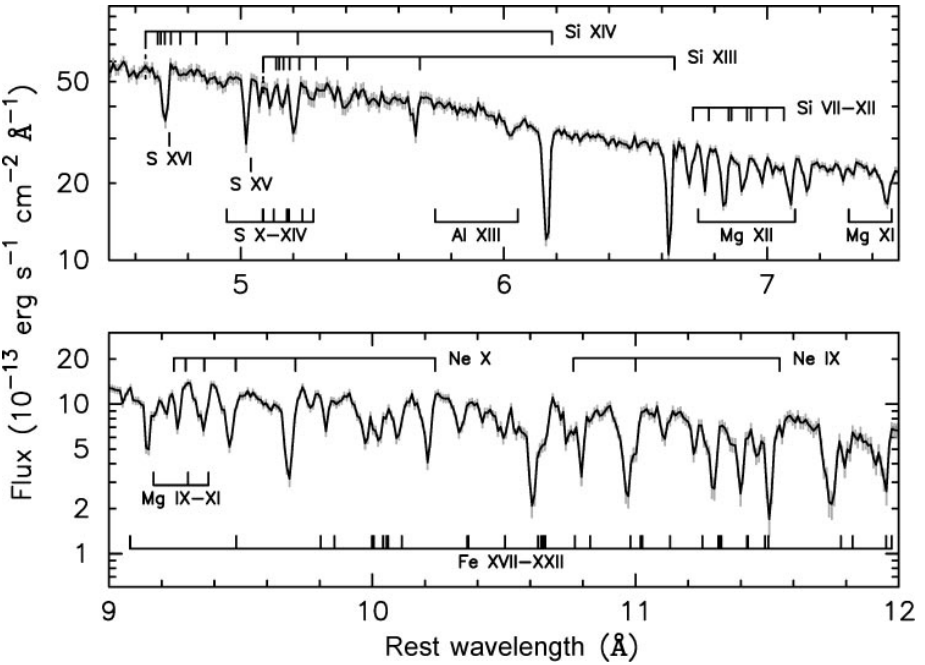

Figure 2 Two parts of the CXO/HEG + MEG spectrum of NGC 3783 (adapted from Kaspi et al. 2002). The upper panel shows the region containing lines due to *K*-shell transitions in Si. For each panel, the locations in the rest frame of the galaxy of the first nine lines in the He- and H-like *K*-shell series are marked (i.e., $n = 1 \rightarrow 2, 3 \ldots$ from right to left), along with the bound/free edges. Many of these lines are clearly detected, as are several lines from less-ionized Si and various Mg, Al, and S ions. The lower panel shows several He- and H-like lines of Ne detected within a forest of lines due to various ionization states of Fe (see Kaspi et al. 2002 for details).

from the "edge fitting" of data from nondispersive instruments (see Section 2.2.1). However, photoionization modeling has already shown that a single zone of absorbing material is unable to reproduce the equivalent widths (EWs) of all the lines observed in several sources, which suggests several zones with different ionization states and possibly different kinematics, as in the UV.

1.2. The History of Intrinsic Absorption

The first nonstellar absorption lines detected in a Seyfert galaxy were seen in optical spectra of NGC 4151 (Oke & Sargent 1968) and found to be due to He I and H I (Balmer) lines that were blueshifted by up to -970 km s^{-1} with respect to the emission lines (Anderson & Kraft 1969), suggesting ejection of matter from the nucleus (see Crenshaw et al. 1999 for more of this early history). Until observations

in the UV and X-rays from space, NGC 4151 provided the only known case of absorption "intrinsic" to a Seyfert galaxy, although intrinsic broad (Weymann et al. 1981) and narrow (Foltz et al. 1986) absorption lines were known to exist in quasars from ground-based observations.

1.2.1. HISTORY OF UV ABSORPTION Early observations of NGC 4151 in the UV, beginning in 1978 with the International Ultraviolet Explorer (IUE), revealed a rich assortment of intrinsic absorption lines spanning a wide range in ionization, from O I to N V, as well as absorption lines arising from excited (i.e., fine-structure and metastable) levels (Boksenberg et al. 1978, Davidsen & Hartig 1978, Penston et al. 1981, Bromage et al. 1985). Bromage et al. found that the absorption-line variations in NGC 4151 are due to changes in the column densities rather than the velocity spread of the clouds. In addition, they suggested that the absorbing region is likely composed of optically thin gas located outside of the BELR. Ulrich (1988) described other Seyfert galaxies that show obvious intrinsic absorption in IUE spectra; most of these showed only Lyα, N V, and C IV absorption, indicating typically higher ionization than that found in NGC 4151.

From a large set of IUE observations, Ulrich (1988) estimated that only 3%–10% of all Seyfert 1 galaxies show intrinsic UV absorption. However, only very strong absorption lines (with $EW > 1$ Å) are detectable at the low resolving power ($R = 200$–400) and low signal-to-noise ratio per resolution element ($S/N < 10$) of an IUE spectrum. With the launch of the HST and its first generation spectrographs (FOS and GHRS) in 1990, the ability to detect intrinsic UV absorption in AGN increased dramatically and led to the discovery that the true percentage of Seyfert 1 galaxies with intrinsic UV absorption is ∼60% (Crenshaw et al. 1999). Furthermore, the high resolution and S/N of the UV observations allow a detailed study of the kinematics and physical conditions of the absorbers. In the UV, this pursuit has been greatly assisted with the installation of the Space Telescope Imaging Spectrograph (STIS) (Kimble et al. 1998, Woodgate et al. 1998) on the HST in 1997; STIS's two dimensional detectors provide echelle spectroscopy at high spectral resolving power ($R = 30{,}000$–$46{,}000$) over a broad wavelength region, which enables simultaneous observations of absorption components in a number of different ions in the UV (cf., Crenshaw & Kraemer 1999). In the far-UV, a limited number of AGN were observed by the Hopkins Ultraviolet Telescope (HUT) (Kruk et al. 1995) at $R = 300$–400 (Kriss 1997). Once again, a great step forward was made possible with the launch in 1999 of the Far Ultraviolet Spectroscopic Explorer (FUSE) (Moos et al. 2000, Sahnow et al. 2000), which operates over the range 912 to 1187 Å and has $R = 20{,}000$ (Kriss 2002).

1.2.2. HISTORY OF X-RAY ABSORPTION With the relatively poor spectral resolving power of X-ray detectors ($R \lesssim 20$ at 1 keV) prior to the launch of the grating spectrometers on board CXO and XMM-Newton, the detection of resonance absorption lines was impossible, and the study of intrinsic absorption was therefore limited to information gained from the broad spectral curvature due to the

superposition of bound/free edges in the soft X-ray band (0.3–3 keV). Nevertheless, it was clear that a large fraction of Seyfert galaxies contained substantial column densities ($N_H \gtrsim 10^{21}$ cm^{-2}) of material (e.g., Lawrence & Elvis 1982). However it was equally clear that the soft X-ray spectra in many sources exhibited a complex spectral form and/or varied in a complex manner (e.g., Warwick et al. 1988, Yaqoob et al. 1989, Arnaud et al. 1985, Turner et al. 1991).

The first observational evidence of X-ray absorption by ionized material was provided by Halpern (1984) using observations by the Einstein Observatory. Halpern suggested that the changing attenuation in the quasar MR2251-178 might be caused by a variable column density of material photoionized by the intense radiation field of the nucleus—a so-called warm absorber. Such an interpretation was supported by subsequent European X-Ray Observatory Satellite (EXOSAT) and Ginga observations of MR2251-178 (Pan et al. 1990, Mineo & Stewart 1993). Other notable EXOSAT and Ginga results include the suggestion of absorption by a warm absorber in the Seyfert 1 galaxies NGC 4151 (Yaqoob et al. 1989) and MCG-6-30-15 (Nandra et al. 1990). Further Ginga observations suggested that many Seyfert 1 galaxies ($\sim$50%) may contain a significant column density ($N_H \gtrsim 10^{23}$ cm^{-2}) of very highly ionized material detected via *K*-shell bound/free edges of Fe XIX–XXVI (Nandra & Pounds 1994). Unfortunately, the low spectral resolution prevented these features from being separated unambiguously from the nearby (broad) Fe $K\alpha$ fluorescence emission (Pounds et al. 1989, 1990; Matsuoka et al. 1990) and the "Compton reflection" continuum (e.g., George & Fabian 1991). However, recent observations with the latest generation of instruments have again revealed evidence for deep absorption features in this region (e.g., Boller et al. 2002). Early pointed-phase observations by the Position Sensitive Proportional Counter (PSPC) on board the Roentgen Satellite (ROSAT) revealed a deficit of photons at $\sim$800 eV in MCG-6-30-15 (Nandra & Pounds 1992) and several other bright Seyfert 1 galaxies (e.g., Nandra et al. 1993; Turner et al. 1993a,b; Pounds et al. 1994) and a radio-quiet quasar (Fiore et al. 1993). This was interpreted as a blend of the O VII (739.3 eV) and O VIII (871.4 eV) bound/free edges. [For a review of X-ray instrumentation prior to the launch of the Advanced Satellite for Cosmology and Astrophysics (ASCA) see Bradt et al. (1992), and for a review of the then-known temporal and spectral characteritics of AGN see Mushotzky et al. (1993).]

With the launch of ASCA (Tanaka et al. 1994) in 1993, the study of intrinsic absorption in the X-ray band took a notable step forward. The Solid-State Imaging Spectrometers (SIS) (Burke et al. 1993) had the resolution and sensitivity to both determine the redshift of the warm absorber to within $\sim 3 \times 10^3$ km s^{-1} and separate the O VII and O VIII bound/free edges. Thus, this detector provided the first real constraints on the ionization state of the warm absorber via the ratio of the depths of these edges. Early observations of MCG-6-30-15 confirmed the warm absorber was indeed at the redshift of the host galaxy, but also revealed the absorber to exhibit changes in opacity on both medium (weeks) and short ($\sim 10^4$ s) timescales. (Fabian et al. 1994, Reynolds et al. 1995, Otani et al. 1996). Early observations of several

other sources also suggested the presence of a warm absorber in some, but not all, sources (e.g., Mihara et al. 1994, Ptak et al. 1994, Weaver et al. 1994, Yaqoob et al. 1994, Guainazzi et al. 1994). By the late 1990s, a sufficient number of objects had been observed by ASCA and BeppoSAX (launched in 1996) that it was clear that $\gtrsim$50% of Seyfert 1 galaxies exhibited soft X-ray spectral features consistent with ionized gas along the line of sight (e.g., Reynolds 1997; George et al. 1998c, and references therein). The column densities derived using a variety of edge-fitting techniques (see Section 2.2.1) for the absorbers covered almost the full accessible range, $N_H \approx 10^{21}$–10^{23} cm^{-2}. Similarly, the absorbers were seen to cover a range of ionization parameters (see Section 3.2).

As discussed in Section 1.1, X-ray spectroscopy of AGN finally became possible with the launch of CXO and XMM-Newton at the turn of the millennium. This new generation of instruments is comprised of the high-, medium-, and low-energy gratings (HEG, MEG, and LEG) (Markert et al. 1994, Brinkman et al. 1997) on board CXO covering (in their first-order spectra) the 0.8–10, 0.4–5, and 0.2–10 keV bands with a (FHWM) $\Delta\lambda \simeq 12$, 23 and 50 m Å, respectively, and the Reflection Grating Spectrometer (RGS) (den Herder et al. 2001) on board XMM-Newton, which covers the 0.3–1.5 keV band and has $\Delta\lambda \simeq 70$ m Å. This new suite of instruments provides resolving powers in the range $R \simeq 200$–1000 at 1 keV.

Table 1 gives a list of the Seyfert 1 galaxies with intrinsic absorption that have published spectra with $R \geq 1000$ in the UV or $R \geq 100$ in the X-ray. Those with nearly simultaneous (within a few weeks) UV and X-ray observations include NGC 3516, NGC 3783, NGC 4051, NGC 4151, NGC 5548, and Mrk 509 (see Table 1 references). Seyfert 1 galaxies that do not show absorption in moderate- to high-resolution spectra can be found in Crenshaw et al. (1999), Gondoin et al. (2001b), Gondoin et al. (2002), and Marshall et al. (2002).

1.2.3. A CONNECTION BETWEEN UV AND X-RAY ABSORPTION? A connection between the UV and X-ray absorbers was made by Mathur et al. (1994) based on ROSAT and HST observations of the quasar 3C 351. Using photoionization models, these authors claimed that a single component of ionized gas could produce both the observed strengths of the O VII and O VIII absorption edges and the equivalent widths of the intrinsic UV absorption lines (O VI, N V, and C IV). Similar claims were made for the quasar 3C 212 (Mathur 1994) and the Seyfert 1 galaxy NGC 5548 (Mathur et al. 1995). However, in some objects, it became clear that multiple components characterized by a wide range in ionization parameter and hydrogen column density were needed to explain the wide range in ionization species and measured column densities; such was the case for NGC 4151 (Kriss et al. 1995) and NGC 3516 (Kriss et al. 1996a,b). Thus, for a number of years, there was a controversy as to whether the intrinsic UV and X-ray absorption features come from the same gas. The resolution of this controversy requires simultaneous UV and X-ray observations at the highest possible spectral resolution, and is described in Section 3.4.

TABLE 1 Seyfert 1 galaxies with intrinsic absorption[a]

Object	Redshift	Type[b]	UV reference	X-ray references
WPVS 007	0.0288	NLS1	Crenshaw et al. 1999 (and references therein)	
I Zw 1	0.0611	NLS1	Crenshaw et al. 1999 (and references therein), Kriss 2002	
Ton S180	0.0620	NLS1	Kriss 2002[c]	Turner et al. 2001[c], 2002[c]
Mrk 359	0.0174	NLS1		O'Brien et al. 2001
NGC 985	0.0431	Sey 1	Kriss 2002	
Ton 951	0.0640	Sey 1	Kriss 2002	
NGC 3227	0.0039	Sey 1	Crenshaw et al. 2001	
NGC 3516	0.0088	Sey 1	Crenshaw et al. 1999 (and references therein), Kriss 2002, Kraemer et al. 2002	Netzer et al. 2002
NGC 3783	0.0097	Sey 1	Crenshaw et al. 1999 (and references therein), Kriss 2002, Kraemer et al. 2001a, Gabel et al. 2003	Kaspi et al. 2000, 2001, 2002; Blustin et al. 2002
NGC 4051	0.0023	NLS 1	Collinge et al. 2001	Collinge et al. 2001
NGC 4151	0.0033	Sey 1	Crenshaw et al. 1999 (and references therein), 2003; Kriss 2002, Kraemer et al. 2001b	Ogle et al. 2000
Mrk 766	0.0129	NLS 1		Branduardi-Raymont 2001, Mason et al. 2002
MCG–06–30–15	0.0077	Sey 1		Branduardi-Raymont 2001, Lee et al. 2001, Sako et al. 2002
IC 4329A	0.0161	Sey 1		Gondoin et al. 2001a
Mrk 279	0.0304	Sey 1	Kriss 2002	
PG 1351 + 64	0.0882	Sey 1	Kriss 2002	
NGC 5548	0.0172	Sey 1	Crenshaw et al. 1999 (and references therein), 2003; Kriss 2002; Brotherton et al. 2002	Kaastra et al. 2000, 2002
Mrk 817	0.0315	Sey 1	Kriss 2002	
Mrk 478	0.0791	Sey 1	Crenshaw et al. 1999 (and references therein)[c], Kriss 2002[c]	Marshall et al. 2002[c]
Mrk 290	0.0296	Sey 1	Kriss 2002	
Mrk 509	0.0344	Sey 1	Crenshaw et al. 1999 (and references therein); Kriss 2000, 2002; Kraemer et al. 2003	Pounds et al. 2001, Yaqoob et al. 2002
II Zw 136	0.0630	Sey 1	Crenshaw et al. 1999 (and references therein)	
Mrk 304	0.0658	Sey 1	Kriss 2002	
Akn 564	0.0247	NLS1	Crenshaw et al. 1999 (and references therein), 2002b; Romano et al. 2002	
NGC 7469	0.0163	Sey 1	Crenshaw et al. 1999 (and references therein), Kriss 2002	

[a]For Seyferts with spectra at $R \geq 1000$ in the UV (900–3200 Å) and $R \geq 100$ at 1 keV in the X-ray.

[b]Sey 1: Normal Seyfert 1 (FWHM[Hβ] $>$2000 km s^{-1}), NLS1: narrow-line Seyfert 1 (FWHM[Hβ] $\leq$ 2000 km s^{-1}).

[c]Intrinsic O VI absorption detected; no intrinsic absorption detected in UV at 1200–3200 Å or in X-ray.

1.3. The Origin of Intrinsic Absorption

Perhaps the most important question to be addressed regarding the intrinsic absorbers is, What is their origin? In other words, how are the absorbers created and, in most cases, accelerated outward from the nucleus? What is their connection to the other components of AGN, and what does this tell us about the overall geometric and dynamical structure of AGN? A related question is, How does the mass outflow affect its environment, including the nuclear regions and host galaxy? There are no clear answers to these questions yet, but there are many clues derived from recent observations and theoretical modeling that are explored in this review. In order to evaluate the significance and reliability of the results in this review, a basic understanding of the techniques for detecting and measuring the absorption, and determining the physical conditions via photoionization models, is needed (Section 2). To investigate the origin of the intrinsic absorbers, their locations need to be known (Section 3); current evidence indicates they are at a variety of positions relative to the central SMBH, including the host galaxy's halo ($\sim$10 kpc), the inner galactic disk (100–1000 pc), the narrow emission-line region (NELR) (10–500 pc), and between the classic BELR and NELR (0.01–10 pc). The physical conditions and kinematics of the absorbers are also needed (Section 3) for comparison with the dynamical models, which invoke origins in the accretion disk, the BELR clouds, the putative torus (used to explain the nuclear obscuration in Seyfert 2 galaxies), or material in the NELR or host galaxy (Section 4). Finally, further improvements are needed in the observational constraints and models before a full understanding of the absorbers and their role in AGN can be achieved (Section 5).

2. ABSORPTION ANALYSIS TECHNIQUES

2.1. Detection

The detection of the absorption lines is very sensitive to spectral resolution, as well as the *S*/*N*. In the UV, IUE ($R = 200$–400) was only able to detect absorption lines with $EW > 1$ Å, due to convolution of the unresolved lines with the surrounding continuum and emission lines. On the other hand, the FOS ($R \approx 1000$) was a much more sensitive detector of absorption; for example, at a $S/N \geq 20$, a typical 3σ detection limit was $EW \approx 0.1$ Å (Crenshaw et al. 1999). Most of the intrinsic absorption lines were still unresolved in FOS spectra, however. Weaker lines can be detected at higher resolution, even at the expense of lower S/N. For example, the 3σ detection limit for GHRS spectra ($R \approx 20{,}000$) at a $S/N \geq 8$ was $EW \approx 0.03$ Å (Crenshaw et al. 1999).

In the X-ray band, the charge-coupled device (CCD) detectors on ASCA had a resolution of $R \approx 12$ in the region of the O VII and O VIII edges, and the study of intrinsic absorption was limited to edge-fitting techniques. The gratings on CXO and XMM-Newton provide over an order of magnitude increase in resolution. For example, at 33.7 Å [$\sim$370 eV in the region of the C VI line (see Section 3.4)] the

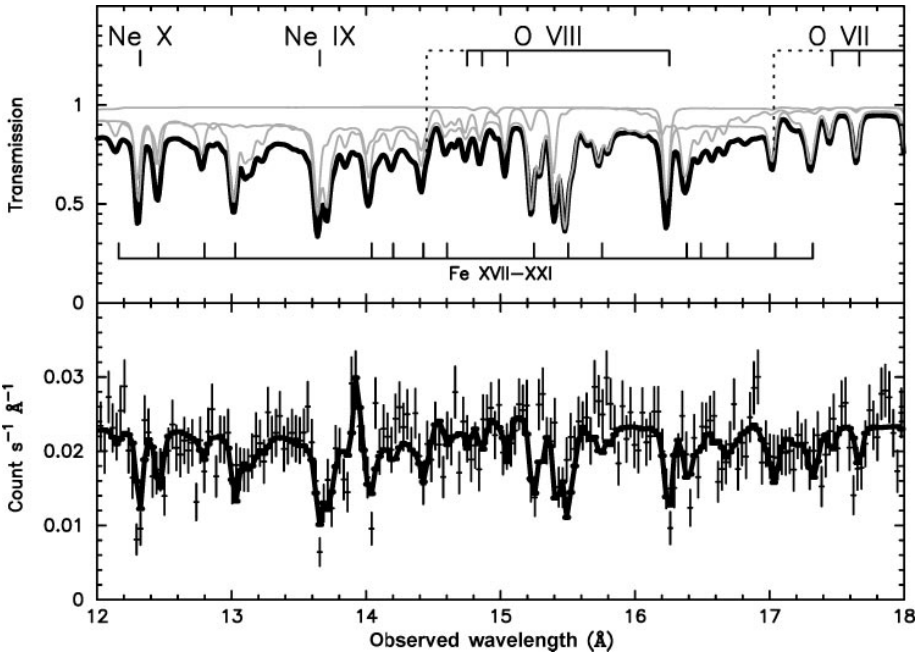

Figure 3 Part of the *CXO*/LEG spectrum of NGC 5548 (adapted from Kaastra et al. 2002). The lower panel shows the data and best-fitting model. The upper panel shows separately the transmission of three warm absorbers implied in this source, along with the total (in *bold*). The He- and H-like lines of O and Ne detected in this region are indicated, along with numerous Fe lines. The dotted lines show the locations of the O VII and O VIII bound/free edges. The prominent emission line visible in the lower panel at 13.9 Å is the Ne IX λ13.700 forbidden line.

CXO/LEG has a resolution of $R \approx 700$, and at 13.4 Å (∼920 eV in the region of the Ne IX triplet), the CXO/HEG has a resolution of $R \approx 1100$. The equivalent velocity resolution of the absorption lines is FWHM $\gtrsim$ 300 km s^{-1}. However, it is the S/N that is generally the limiting factor. This is clearly illustrated in Figure 3, obtained from a typical ∼90 ks observation of NGC 5548, one of the brightest Seyfert 1 galaxies. Given a $S/N \lesssim 3$ in the overlying continuum, the *EW* of the C VI line can only be constrained to 90 $\pm$ 30 mÅ, and the radial velocity to -430 ± 120 km s^{-1} (Kaastra et al. 2002). The CXO/LEG has more collecting area at higher energies, as does the XMM-Newton/RGS around the C VI line, and thus higher *S*/*N* can be achieved at the cost of lower spectral resolution.

Superior resolution is available using the CXO MEG and HEG gratings. The data illustrated in Figure 2 has $S/N \approx 20$ and 10 in the MEG and HEG, respectively, and the *EW*s of approximately 100 lines can be measured at $\gtrsim 3\sigma$ confidence (Kaspi et al. 2002). However, these data were obtained by coadding 10 days of CXO observing time on NGC 3783. Thus, the quality of the data obtained from

this source is far superior to that from other Seyfert 1 galaxies observed to date. As can be seen from Figures 2 and 3, and figure 10 of Kaspi et al., although the lines are clearly broader than the instrumental response, they are far from being resolved. While yet better resolution is provided by the higher-order spectra, the *S/N* is at least an order of magnitude lower, limiting the usefulness of these data.

2.2. Absorption Measurements

2.2.1. EDGE FITTING With X-ray data from detectors with low or medium spectral resolution, the study of absorption relies on bound/free electron transitions. However, the combination of limited *S/N* and the spectral resolution of most instruments flown to date, the relevant atomic cross-sections, and Galactic absorption usually limits this technique to column densities in excess of $N_H \sim 10^{20}$ cm^{-2}. Fortunately, in many Seyfert 1 galaxies, substantially higher columns are present, most noteably in H- and He-like ions of the abundant elements. This results in deep energy-dependent "edges" in the observed spectrum at the thresholds for photoelectric absorption (E_{th}) followed by a relatively slow [$(E/E_{th})^{-n}$, with $n \approx 3$] decrease in opacity (e.g., Verner & Yakovlev 1995, Verner et al. 1996). Generally, one of two techniques have been employed (e.g., see Reynolds 1997; George et al. 1998c, and references therein). The first is the addition of a series of photoelectric absorption edges to some broad continuum until an acceptable model is obtained. One can then attempt to derive the ionization parameter (Section 2.3.1) from the best-fitting values of *N* (ion) and continuum shape. The second is by computing synthetic spectra from a grid of photoionization models and fitting the observed spectra to simultaneously derive the ionization parameter, N_H, and the continuum.

2.2.2. UNRESOLVED LINES When the instrumental resolution is similar to or exceeds the intrinsic widths of the lines, one must resort to the curve of growth (COG) method, which describes the increase in the EW of an absorption line as the column increases (Spitzer 1978), or a line-fitting routine in which the instrumental profile is convolved with an assumed intrinsic profile and fit to the observed absorption. The two methods are similar in that they assume an underlying distribution of velocities or intrinsic profile (e.g., Gaussian or Voigt). Because one does not know the intrinsic profile a priori, this assumption can be dangerous, although it has been used with success for ISM lines. For both techniques, the intrinsic width is used as a free parameter and is often characterized by the velocity spread parameter "*b*" (Spitzer 1978); for a Gaussian, the dispersion $\sigma = b/\sqrt{2}$, and FWHM $= 1.67b$.

If there are enough lines from the same ion, the COG method can be used to estimate the ionic column density directly. For example, the EWs of the O VII lines from the CXO spectrum of NGC 5548 (Kaastra et al. 2002) are plotted along the y-axis in Figure 4 (*left panel*). The points were shifted along the x-axis until they matched a COG with a particular *b* value, and their final positions give the column density of O VII. The parameters derived from the COG are $N(O\ \text{VII}) = 4.0\ (\pm 1.5) \times 10^{17}$

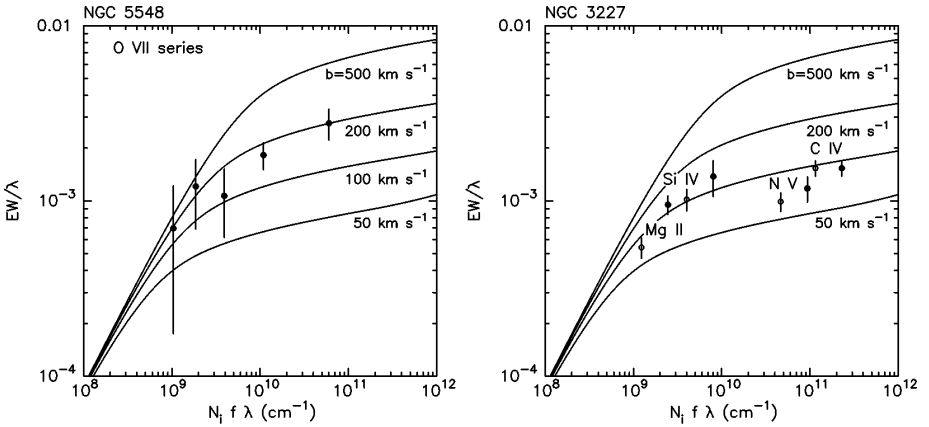

Figure 4 Left panel: Curves of growth based on the equivalent widths of O VII absorption lines in the CXO spectrum of NGC 5548 (Kaastra et al. 2002). A good match is obtained for N(O VII) $= 4.0\ (\pm 1.5) \times 10^{17}$ cm^{-2} and $b = 200\ (\pm 50)$ km s^{-1}. Right panel: Curves of growth based on the equivalent widths of absorption lines in NGC 3227 and predicted column densities from the photoionization models in Crenshaw et al. (2001). The *EW*s of the absorption lines are consistent with the models for a b value of 100 ± 50 km s^{-1}.

cm^{-2} and $b = 200\ (\pm 50)$ km s^{-1}; the column is essentially the same as that derived by Kaastra et al. (2002) from directly fitting the spectrum.

If there are only a few absorption lines available, which is typical in the UV, then the COG method can be used to see if the EWs are consistent with the column densities produced from a model (e.g., Kriss et al. 1996a). For example, Figure 4 (*right panel*) shows this method for the measured *EW*s of lines from different ions in a low-resolution STIS spectrum of NGC 3227 (Crenshaw et al. 2001) and plotted against the ionic column densities from a previous photoionization model (derived independently from the X-ray data, see Kraemer et al. 2000b). The plot shows that the measured *EW*s are consistent with the model columns at a *b* value of 100 ± 50 km s^{-1}.

2.2.3. RESOLVED PROFILES The most reliable measurements are those from fully resolved profiles, which permit the direct determination of ionic column densities, radial velocity centroids, and FWHMs of the components. Resolved profiles are only currently available in UV spectra at $R \gtrsim 20{,}000$. The standard method of analysis is to produce a normalized absorption profile by dividing the spectrum by the continuum plus emission-line fit. In contrast with studies of interstellar absorption lines, an allowance is made for partial covering. The covering factor in the line of sight (C_f) is the fraction of light that is occulted by the absorber and can, in principle, be a function of v_r. In the case where $C_f = 1$ (e.g., for ISM lines), the optical depth at each radial velocity is given by $\tau = -\ln(I_r)$ (Spitzer 1978), where I_r is the normalized residual flux at that radial velocity.

For $C_f < 1$, the optical depth at a particular v_r is given by

$$\tau = \ln\left(\frac{C_f}{I_r + C_f - 1}\right) \quad (1)$$

(Hamann et al. 1997c). The ionic column density is then obtained by integrating the optical depth across the profile:

$$N = \frac{m_e c}{\pi e^2 f \lambda} \int \tau(v_r)\, dv_r \quad (2)$$

(Savage & Sembach 1991), where λ is the wavelength and f is the oscillator strength (Morton et al. 1988). Blending of lines from different kinematic components can cause problems (see Figure 1), but can be compensated for by using optical depth templates derived from unblended lines (Kraemer et al. 2001a), or by fitting the components (e.g., with Gaussians) in optical depth (Espey et al. 1998).

2.2.4. COVERING FACTORS AND SATURATION For intrinsic absorption, $C_f < 1$ could be the result of sources of unocculted emission that lie inside the projected aperture but outside of the absorption region, or true partial covering of the background emission by the absorbers. Potential sources of unocculted emission in the aperture include (*a*) a scattering region outside of the absorber that reflects continuum and BELR emission into the line of sight (Kraemer et al. 2001b), (*b*) NELR gas outside of the absorbers (Kraemer et al. 2002), or (*c*) UV and/or X-ray sources in the host galaxy (such as a starburst). True partial covering of the background emission can occur due to small clouds, for example, or a flow which only partially occults the background emission.

Partial covering has a strong impact on the absorption-line measurments in that it can make a saturated line appear unsaturated. For example, the broad absorption lines of BAL quasars seldom reach zero intensity, and it is now clear that this is due to uncovered light in their troughs (Arav 1997, Hamann & Ferland 1999). Prior to this realization, BAL column densities were severely underestimated, which resulted in, for example, peculiar (and incorrect) values for the abundances in these regions (see Hamann & Ferland 1999). Spectropolarimetry indicates that in many cases, the light in the BAL troughs is polarized and therefore comes from a scattering region (e.g., electrons or dust) that lies outside of the absorption region as projected onto the sky (Goodrich & Miller 1995).

Fortunately, there are techniques for deriving covering factors in the cores of absorption lines from high-resolution spectra, and for spectra with a high *S*/*N*, they can be determined as a function of v_r. For any absorption line, a lower limit to C_f is simply $C_f \geq 1 - I_r$. If a line is known to be completely saturated, then the above limit becomes an equality over the range of saturation. In the extreme case where the line is completely saturated over all radial velocities, then $C_f(v_r)$ is just specified by the profile $I_r(v_r)$ (Arav et al. 1999, Gabel et al. 2003), but only a lower limit can be derived for the ionic column density.

Usually, the degree of saturation cannot be estimated a priori. Fortunately, C_f can be determined from a multiplet if the ratios of optical depths for the lines are fixed by their oscillator strengths. For a resonance doublet, if the true ratio of the optical depths is 2 (e.g., the O VI, N V, C IV, and Si IV doublets), then

$$C_f = \frac{I_1^2 - 2I_1 + 1}{I_2 - 2I_1 + 1}, \tag{3}$$

where I_1 and I_2 are the residual normalized fluxes in the weaker line (e.g., C IV λ1550.8) and stronger line (e.g., C IV λ1548.2), respectively (Hamann et al. 1997c). Although the doublet technique is very useful, there is a hidden assumption that the uncovered emission is a constant fraction of the continuum plus emission-line fit, which is not always the case. For example, if the red member of an absorption doublet is sitting on top of substantial emission from the NELR, and the blue member is not, then one could obtain an erroneous value for C_f unless this effect is properly accounted for (Kraemer et al. 2002, Arav et al. 2002b, Crenshaw et al. 2003). As another example, the spectrum of reflected radiation can be different from that of the continuum plus emission-line fit because it depends on which emission and absorption components are inside of the scattering region (Kraemer et al. 2001b).

In the case of true partial covering of the background emission, it is possible to have different covering factors for the continuum source (C_f^c) and BELR (C_f^l) due to the different projected sizes of these regions. Assume that the same column of gas is in front of both emission sources (i.e., $\tau = \tau_l = \tau_c$). Following Gabel et al. (2003) (see also Ganguly et al. 1999), the normalized flux in the absorption line is given by

$$I_r = R_l\left(C_f^l e^{-\tau} + 1 - C_f^l\right) + R_c\left(C_f^c e^{-\tau} + 1 - C_f^c\right), \tag{4}$$

where R_l and R_c are the fractional contributions of line and continuum emission to the total emission. The effective covering factor in the line of sight is then given by $C_f = R_l C_f^l + R_c C_f^c$, which can be used in Equation 1 for determining the optical depth as a function of v_r. This technique has been applied to high *S*/*N* spectra of NGC 3783 obtained with STIS and FUSE to obtain separate continuum and BELR covering factors across the profiles of several components; the results are discussed in Section 3.1.3.

2.3. Photoionization Models

2.3.1. BASICS There is general agreement that the outflowing gas observed in absorption in AGN is photoionized by the central source; hence, the physical conditions within the absorbers are typically constrained using photoionization models. It is usually assumed that the absorber is far enough from the central source that it can be modeled as an infinite (in the transverse plane) slab of gas. The models generally assume constant density through the slab, with the gas in a state of thermal equilibrium. The ionization and thermal structure is determined at each

point within the gas along a radial direction from the illuminated face of the slab (hence, from the central source). This will produce a depth-dependent opacity at each frequency, as well as the emission coefficients for different lines and continua. Several photoionization codes exist and have been used in the analysis of intrinsic absorption, including Cloudy (Ferland et al. 1998), Ion (Netzer 1990), and Xstar (Kallman & Bautista 2001).

Although the actual calculations performed within the code while generating a model can be quite complex (for some of the details, see Rees et al. 1989), the result is contained in two physical quantities: the total column density of the slab and its state of ionization. The former is given as the total hydrogen column density, $N_H = N_{HI} + N_{HII}$, and the latter is parameterized in the form of the ionization parameter. Two equivalent definitions of the ionization parameter are used: (*a*) the number of ionizing photons per nucleon at the ionized face of the slab,

$$\mathrm{U} = \int_{\nu_0}^{\infty} \frac{\mathrm{L}_\nu h\nu}{4\pi r^2 nc}\, d\nu, \tag{5}$$

where L_ν is the ionizing luminosity per frequency interval above the Lyman limit, r is the distance to the central source, n is the number density of the gas at the ionized face of the slab (either the number density of hydrogen nuclei or free electrons), and $h\nu_0 = 13.6$ eV, and (*b*) $\xi = \frac{\mathrm{L}}{nr^2}$, where L is the total ionizing luminosity. One can easily convert between U and ξ for a given spectral energy distribution (SED) of the ionizing continuum. Alternatively, another form of the ionization parameter is the ratio of photon pressure to the gas pressure (or "pressure ionization parameter") $\Xi = L/(4\pi r^2 c\mathrm{p})$, where p is the gas pressure. Converting between the standard ionization parameters and the pressure ionization parameter requires calculating the mean electron temperature within the gas, which strongly depends on the SED and the gas density.

For absorption studies, the modeling methodology consists of varying U and N_H until the predicted ionic column densities match those determined through the measurements of the depths of absorption lines and/or bound-free edges. Among the model inputs are the SED, the elemental abundances, and the fraction of cosmic dust. The density of the gas is also an input; however, the predicted ionic column densities are relatively insensitive to density for $n_H < 10^{10}$ cm^{-3}. Codes permit the specification of the turbulent velocity within the gas, which may affect the predicted ionization structure in cases of optically thick, highly turbulent gas (which is not typically the case for UV absorbers).

The exact nature of the SED in AGN is not well known, particularly in the extreme ultraviolet (EUV) at the ionization energies of many of the ions detected in UV absorption. The veracity of the prediction that the UV and X-ray absorption arises in the same component (e.g., Mathur et al. 1995, 1997; Crenshaw & Kraemer 1999; Kriss et al. 2000) may depend strongly on the choice of SED because the fraction of Li-like ions such as C IV and N V in an X-ray absorber with large O VII and O VIII columns depends on the ratio of the flux at energies above and below ~100 eV. Given the ratio of UV to X-ray flux and hardness of the

nonionizing UV continuum, it is certain that the continuum must turn down at energies above the Lyman limit in order to meet the X-ray continuum. A typical approach has been to fit power laws to the observed UV and X-ray continua and join the two in the unobservable EUV with a single power-law, with a typical spectral index of $\alpha_\nu \approx 1.5$. Although this approach generally provides a good match to the observed ionic columns, the reality may be more complicated. For example, in order to overcome an apparent deficit in photons above the He II Lyman limit (54.4 eV) Mathews & Ferland (1987) proposed an SED that peaks in the UV, i.e., the "big blue bump." However subsequent observations of intermediate redshift quasars (Zheng et al. 1997, Laor et al. 1997) indicated a turn-over much closer to the Lyman limit. To complicate matters, observations of narrow-line Seyfert 1 s [(NLS1s) characterized by FWHM[Hβ] ≤ 2000 km s^{-1}] indicate a steep rise in the soft-X-ray band (Boller et al. 1996), which may be thermal in origin (e.g., Turner et al. 2001). Further work is needed to determine if photoionization models of the absorbers can actually be used to constrain the SEDs of different types of AGN.

The physical conditions in the absorbers, and the photoionization modeling, can be complicated if an absorber is screened from the continuum source by intervening gas (e.g., Kraemer et al. 2002), particularly if the intervening gas is optically thick to the ionizing radiation; hence the SED must be modified to account for the intervening absorption. Furthermore, when modeling the physical state of the gas in higher flux states, one must also modify the SED to account for both the increase in the source luminosity and accompanying drop in the opacity of the screen. In extreme cases, the screened gas may become so highly ionized as to be undetectable during high flux states (Kraemer et al. 2001b, 2002).

Solar abundances (e.g., Grevesse & Anders 1989) are generally assumed as a starting point, although there are indications of supersolar abundances in quasars (Section 2.3.2). Even modestly supersolar abundances of particular elements (e.g., nitrogen) will affect the model predictions. Although dusty X-ray absorbers have been considered (e.g., Brandt et al. 1996), it is only recently that the possibility of dust within the UV absorbers has been discussed (Crenshaw et al. 2001, 2002b; de Kool et al. 2001). The main effect of the dust is the depletion of certain elements from the gas phase into the dust grains (principally C, Mg, Si, and Fe), although the screening of the continuum and photo-electric heating by dust grains can be an important effect in optically thick gas (see Ferland et al. 1998). It is hard to constrain the dust/gas ratio within the absorbers with column densities $N_H < 10^{20}$ because the amount of dust extinction will be quite small, and likely undetectable.

As noted by Netzer (1993), the photoionization codes may be incomplete because not all physical processes are included. It is critical that the most accurate atomic data, including recombination rates, ionization cross-sections, charge exchange rates, and Auger yields, be included. For example, there have been no calculations of dielectronic recombination rates for third-row elements beyond silicon, although there have been attempts to approximate these rates (Ali et al. 1991). The absence of these data casts some doubt on the predicted ionization balance of abundant elements, such as iron.

Because the absorbers respond to changes in the ionizing continuum, it is clear that time-dependent effects must be important. Nicastro et al. (1999b) attempted to study the changes in the ionization state of gas exposed to a time-varying continuum source by generating a set of models for different ionization equilibria using the formulation for equilibration times suggested by Krolik & Kriss (1995). However, there have been no detailed calculations of the time evolution of the gas in response to continuum changes, particularly in cases where the gas may not have had time to equilibrate.

As discussed by Krolik et al. (1981), photoionized gas can exist in two regimes of thermal equilibrium (the exact conditions are quite sensitive to the SED): (*a*) when the ionization state of the gas is low enough that there is a balance between heating by ionization and cooling by collisionally excited emission lines and (*b*) at very high ionization, when thermal equlilibrium is established between Compton and inverse Compton processes. At intermediate values of U and T, the gas will undergo large temperature fluctuations in response to changes in the ionizing flux and may be unstable to such perturbations. Figure 5 shows a schematic representation of

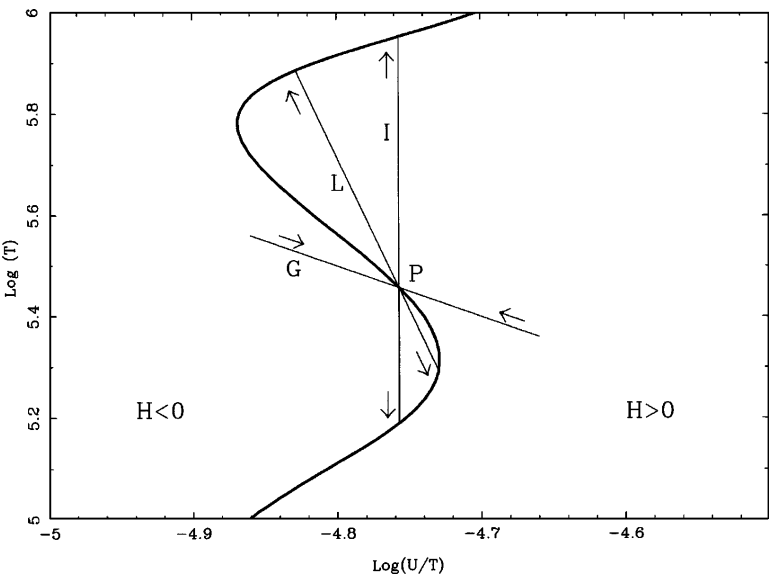

Figure 5 Schematic depiction of an unstable (to isobaric perturbations) portion of an *S* curve (from Bottorff et al. 2000). The regions marked H <or> 0 are those where the cooling rate in the gas is greater than or less than the heating rate. Different perturbation paths (marked G, L, and I) are shown crossing the point P. Arrows show the direction gas will evolve along a constraint when perturbed off the point P. Path I corresponds to a thermally unstable isobaric perturbation. Path L has a slope less than the *S* curve at point P, hence; perturbations constrained on this path are unstable. Path G has a slope greater than the *S* curve at P; hence, perturbations constrained to this path are stable.

an unstable (to isobaric perturbations) portion of a so-called **S** curve (a plot of T versus U/T; the latter is equivalent to Ξ, the pressure ionization parameter). Intrinsic absorbers span a large range in ionization parameter and temperature, even in the same galaxy (see, for example, the case of NGC 3783; Kraemer et al. 2001a, Kaspi et al. 2001). Also, individual components of absorption may undergo dramatic changes in response to changes in the ionizing flux (Kraemer et al. 2001b, 2002; Netzer et al. 2002). Hence, some of the absorbing gas may be unstable (or semistable; see Krolik & Kriss 2001) to thermal perturbations. In fact, it is possible that fluctuations can produce a two-component gas in which a Compton-heated medium can give rise to low ionization knots (Krolik & Kriss 1995, 2001).

2.3.2. MODELING THE ABSORBERS In high-resolution UV spectra, the ionic column densities of individual kinematic components can be modeled. The basic approach is to vary U and N_H until the model predictions for the column densities match those observed to within the measurement errors. Fitting the ratios of two ions of sufficiently different ionization potentials will provide a unique solution; the ratio of N V/C IV is particularly sensitive to U and N_H because the ionization potential to create N V is above the He II Lyman limit and C IV is below it, and the relative amounts of N V and C IV depend on the fraction of the slab that is optically thin at the HeII Lyman limit. Because there is always some neutral hydrogen, comparison of an ionic column density from a relatively high ionization species (e.g., C IV, N V, or O VI) to that of H I can yield two solutions: (*a*) a high ionization solution, with a large column of gas containing a trace of H I, and (*b*) a low ionization solution, with a relatively small column of gas, truncated to keep the H I column low (see Brotherton et al. 2002). The presence or absence of lower ionization states, such as C II and O I, and those from elements with lower abundance, typically Si IV and Mg II but occasionally rarer species such as P V (Kraemer et al. 2001b, Gabel et al. 2003), can be used to constrain the models, particularly in cases where the lines from the more commonly detected ions are saturated (Kraemer et al. 2001b, Arav et al. 2002b).

Even with the vast improvements provided by CXO and XMM-Newton, X-ray spectra generally lack the resolution to identify the individual kinematic components detected in the UV spectra. Hence, the X-ray models are limited by the fact that the absorption features may arise in several zones with a large range in physical conditions. Nevertheless, the approach for photoionization modeling is essentially the same as that used for the UV absorbers. The standard definition of U includes the integral photon flux per unit density above 13.6 eV. The large drop in the number of photons emitted per unit frequency interval between 13.6 eV and the X-ray band for the SED of all AGN (excluding certain classes of blazars) results in the standard U (or ξ) being dominated by low-energy photons. However, these photons have insufficient energy to participate in K-shell processes within ions detectable in the X-ray band and hence are of little consequence to X-ray observations. Thus, a number of other definitions have been used within the X-ray community. These include U_X, defined as the 0.1–10 keV photon flux per unit

density (Netzer 1996), and $U_{\rm oxygen}$, which further restricts the energy range of the photon flux to between 538 eV (the O I K-shell edge) and 10 keV (George et al. 2000).

As with the UV analysis, U and N_H can, in principle, be obtained from two ions of the same element (O VII and O VIII are often used—see Section 2.2.1). However, some complications have arisen in the modeling of X-ray absorption. Several sources observed with ASCA and BeppoSAX exhibited a deficit of observed photons at ∼1 keV compared to the otherwise seemingly acceptable photoionization models. This was interpreted as evidence for at least one more absorbing "cloud/system" (sometimes referred to as zone), with a higher ionization parameter, along the line of sight (e.g., George et al. 1998b) and/or a blend of resonant absorption lines involving the excitation of L-shell electrons in Fe (e.g., Nicastro et al. 1999a). In addition, XMM-Newton/RGS and CXO spectra of several objects contain an unresolved transition array (UTA) due to $2p \rightarrow 3d$ transitions in Fe VII–XII. As noted by Sako et al. (2001), this feature occurs in the 730–780 eV ($\lambda \simeq$ 16–17 Å) band and hence could be misidentified as an O VII bound/free edge (739 eV). Clearly, the theoretical and observational ambiguities are greatly reduced the larger the number of species considered.

3. CONSTRAINTS ON THE OUTFLOWING ABSORBERS

Valuable constraints on the outflowing absorbers in AGN have been obtained from the spectra and photoionization models described in the previous sections. These constraints are crucial for understanding the structure of the absorbing regions and the dynamical forces at work, and eventually discriminating between the various dynamical models described in Section 4.

3.1. Geometric and Kinematic Constraints

3.1.1. FREQUENCY OF OCCURRENCE The fraction of AGN that show intrinsic absorption (F) is important for understanding the overall geometry of the absorption regions. For Seyfert 1 galaxies, surveys in the UV (Crenshaw et al. 1999), FUV (Kriss 2002), and X-rays (Reynolds 1997, George et al. 1998c) find that F is in the range 0.5–0.7 for both UV and X-ray absorbers; a naïve average of these values gives $F = 0.6 \pm 0.1$. For quasars, the fraction of occurrence has been found to be similar or slightly lower. Ganguly et al. (2001) find $F = 0.25$ for "associated" C IV absorption lines (within 5000 km s^{-1} of the emission-line redshift) in $z < 1.0$ quasars, and George et al. (2000) find $F = 0.3$ for X-ray (O VII and O VIII) absorption in mostly low-z quasars (although bandpass limitations and low S/N have prevented definitive statements on the latter) (George et al. 2000, Reeves & Turner 2000). However, Laor & Brandt (2002) obtain $F = 0.50$ for C IV absorption in $z < 0.5$ quasars, and Vestergaard (2003) obtains $F = 0.55$ for C IV in quasars over the range $1.5 < z < 3.5$, where the latter study shows nearly equal fractions of occurrence for radio-loud and radio-quiet quasars. Thus, intrinsic UV and X-ray

absorption is prevalent over a wide range in luminosity, occuring in about half of these AGN, and while there is some evidence that the fraction of occurrence may be lower for low-redshift quasars, further study is needed to characterize any trends. An important note of caution is that in quasars, a portion of the detected absorbers could be intervening rather than intrinsic; for example, Ganguly et al. (2001) estimate that of the 15 absorption-line systems they detect, ∼5 are statistically expected to be intervening.

At the low end of the AGN luminosity scale, low-ionization nuclear emission-line regions (LINERs) often show absorption lines in the UV, but these likely arise from the host galaxy ISM, and there is no strong evidence for outflowing gas (Shields et al. 2002). This may be due to insufficient power to drive the outflows or to a different accretion structure from which the outflows may arise (Shields et al. 2002). The only known case for intrinsic absorption in a low-luminosity AGN is for NGC 4395, which is a Seyfert galaxy with $L_{bol} = 10^{41}$ ergs s^{-1}, but with emission-line ionization parameters similar to those of normal Seyferts (Kraemer et al. 1999). NGC 4395 shows evidence for both blueshifted C IV absorption (Filippenko et al. 1993) and ionized X-ray absorption (Moran et al. 1999, Iwasawa et al. 2000) that are intrinsic to its nucleus. Further observations of low-luminosity AGN are needed to understand the parameters that determine the occurrence of intrinsic absorption.

3.1.2. GLOBAL COVERING FACTOR The global covering factor (C_g) is the fraction of emission intercepted by the absorber averaged over all lines of sight, and it can be determined in one of two ways. It can be determined statistically from a sample of AGN of the same type, such that

$$C_g = \langle C_f \rangle F, \tag{6}$$

where $\langle C_f \rangle$ is the average over all objects of the covering factor in the line of sight from the deepest component in each object. For the UV absorbers in Seyfert 1 galaxies, Crenshaw et al. (1999) find that $F = 0.59$ and $\langle C_f \rangle \geq 0.86$, which leads to $C_g \geq 0.51$. There are two extreme possibilities: (*a*) $C_g \approx 0.5$ in all Seyfert 1 galaxies, or (*b*) $C_g \approx 1.0$ in half the objects, with the remaining half having no absorbing gas. The actual situation is likely to be somewhere in between. X-ray absorbers also have large covering factors in the line of sight, which indicate a similar C_g of ∼0.5. Thus, the absorbing regions subtend a very large solid angle, regardless of whether they consist of large contiguous sheets or flows, or ensembles of small clouds. If Seyfert 1 galaxies are seen at preferred viewing angles [e.g., inside the bicone of ionized gas postulated by unified models (see Antonucci 1993)], then the derived values of C_g are with respect to the solid angle over which they are observed.

The other way to determine C_g is to identify emission lines associated with the absorption regions and compare their strengths to those predicted from photoionization models assuming full coverage of the continuum source. The ratio of observed to predicted strengths then gives C_g directly for a given source. CXO spectra

of several objects show emission lines (mostly from O and Ne—see Section 1) that likely arise in the X-ray absorber and yield $C_g = 0.5$–1.0 for each source, which is in agreement with the statistical approach.

3.1.3. COVERING FACTOR IN THE LINE OF SIGHT C_f gives important information on the clumpiness of the absorbing region and/or the nature of any unocculted emission. Values for the deepest component in a Seyfert 1 galaxy range from 0.5 to 1.0 (Crenshaw et al. 1999), and the full range of values extends from (the typical detection limit of) 0.2 to 1.0 for Seyfert 1 galaxies and quasars (e.g., Hamann et al. 1997b,c, 2001; Ganguly et al. 1999). In Mrk 509 (Kraemer et al. 2003) and NGC 3783 (Gabel et al. 2003), the covering factors reveal evidence for at least two subcomponents with different ionization parameters within a single kinematic component. In both objects, the Si IV doublet yields $C_f \approx 0.3$, whereas it should be $\sim$1.0 and $\sim$0.7 for Mrk 509 and NGC 3783, respectively, based on covering factors derived from the C IV and N V doublets. If these subcomponents are at the same location, which is a reasonable assumption given their shared kinematics, then the Si IV absorption comes from compact clouds with higher densities (from the lower ionization parameters; see Equation 5) than the surrounding high-ionization gas. Additional evidence for clumpiness comes from evidence that C_f can vary across the absorption profile in a way that cannot be explained by scattered light. For NGC 3783, Gabel et al. (2003) have determined separate covering factors for the continuum (C_f^c) and BELR (C_f^l) as a function of v_r for three kinematic components of absorption; they find that $C_f^c \geq C_f^l$ at each v_r and that both decrease from the core to the wings of each component. This suggests a clump of clouds traveling outward at the same approximate velocity but with some dispersion, so that the number of clouds decreases from the core to the wings. One of the most surprising observations to date are those of the narrow absorption lines in the quasar 3C 191, which show evidence for partial covering at a large distance (28 kpc) from the nucleus (Hamann et al. 2001); it is difficult to understand how the small clouds have maintained their integrity over the outflow timescale of $\sim 3 \times 10^7$ year. Finally, in the Seyfert 1 galaxy NGC 4151, partial covering is more likely due to unabsorbed scattered light, similar to the situation for BAL quasars; this is discussed in more detail in Section 3.3.

3.1.4. TRANSVERSE SIZE AND VELOCITY A lower limit to the transverse (across the line of sight) size of an absorption component is simply $d_T \geq d_l \sqrt{C_f^l}$, where d_l is the diameter of the source of background light. In the UV, this is the BELR, whose size has been determined for many Seyfert galaxies and some quasars by the process of reverberation mapping (Peterson & Wandel 2000). In the X-ray, the background emission is from the X-ray continuum, which is typically assumed to be ct_{var}, where t_{var} is some continuum variability timescale. As a typical example, the size of the N V emitting region in NGC 5548 is $d_l \sim 4$ light days (Korista et al. 1995, Clavel et al. 1991) and the covering factor for component 3 (Figure 1) is $C_f \approx 0.7$ (Crenshaw et al. 2003), so $d_T \geq 3.4$ light days (8.8×10^{15} cm).

Crenshaw & Kraemer (1999) found that the hydrogen column density of this component varied substantially over ∼19 months, indicating bulk motion of gas across the line of sight. This is an upper limit to the crossing time Δt, so a lower limit to the transverse velocity for this component is $v_T \geq d_T/\Delta t \geq 1700$ km s^{-1}, which is somewhat larger than its radial velocity of $v_r = 540$ km s^{-1}. A few other measurements of v_T have yielded similar lower limits, comparable to the radial velocities (Maran et al. 1996; Kraemer et al. 2001a,b). Many other absorption components monitored on a yearly basis have not shown significant column changes, which indicates that the transverse velocities could be much lower for these components (e.g., several components in NGC 5548) (Crenshaw et al. 2003).

3.1.5. RADIAL VELOCITY AND FWHM In the UV, the radial velocity centroids (v_r) of absorption components in Seyfert 1 s range from +200 to −2100 km s^{-1} (Crenshaw et al. 1999, Kraemer et al. 2003). The few positive values detected are probably not cases of infall, but rather a result of (*a*) measuring the velocities with respect to the narrow emission lines, which tend to be slightly blueshifted with respect to the galaxy's H I 21-cm emission (Crenshaw et al. 1999), and/or (*b*) an origin in the host galaxy's halo. Radial velocities as high as −2400 km s^{-1} have been detected in X-ray absorbers (Collinge et al. 2001). Quasar narrow absorption lines (NALs) also show a broad range of v_r extending up to much higher velocities than in Seyferts (Ganguly et al. 2001, Vestergaard 2003). Hamann et al. (1997a) describe an intrinsic absorption system in PG 0935 + 417 at an ejection velocity of −51,000 km s^{-1}, which is similar to the maximum radial velocities seen in BAL quasars (Weymann et al. 1981). Further discussion on correlations between velocity and luminosity can be found in Section 3.6.

The UV absorbers also show a broad range in widths, from 20 to 500 km s^{-1} (FWHM) in Seyfert 1 s, indicating turbulence, a strong outflow velocity gradient, or superposition of subcomponents. High-resolution spectra of quasars show similar systems in the form of NALs, but also the BALs with widths that extend up to ∼10,000 km s^{-1} (Weymann et al. 1981). Notably, BALs are not found in Seyfert 1 galaxies, which suggests a dependence of velocity dispersion (or at least the maximum possible value) on luminosity. As discussed in Section 3.4, X-ray absorption lines are often slightly broader than the instrumental resolution in CXO spectra, but it is not clear if these are truly broad or just blends of unresolved components.

3.2. Physical Constraints

3.2.1. IONIZATION PARAMETER AND COLUMN DENSITY The ionization parameters derived from photoionization modeling of the ionic columns in UV absorbers span a large range, $\log(U) \approx -4.0$ to 0.0, reflecting a wide range of ionic species, even within an individual AGN (e.g., O I to O VI in NGC 4151) (Kraemer et al. 2001b; Kriss et al. 1992, 1995). Not surprisingly, the X-ray absorbers extend this range

to higher values: $\log(U) \approx -1.4$ to 1.0 (e.g., NGC 5548) (Kaastra et al. 2002). On average, the UV, and particularly the X-ray, absorbers are more highly ionized than the BELR and NELR, which typically have values in the range $\log(U) \approx -3.0$ to -1.0 (Osterbrock 1989).

The hydrogen column densities also span large ranges: $\log(N_H/\mathrm{cm}^{-2}) \approx 18.0$ to 21.5 for the UV absorbers and 21 to 23 for the X-ray absorbers. The low ends of these ranges are likely determined by limits in telescope/detector sensitivities, and the high ends could be affected by saturation of the absorption lines or edges, particularly in the lower-resolution X-ray data. BAL quasars show evidence for even higher UV column densities, and the X-ray columns in particular can reach $\log(N_H) \approx 24$ (e.g., Green et al. 2001; Gallagher et al. 2002, and references therein); at greater values the column of gas starts to become Compton thick (given the Thomson cross-section, $\sigma_T = 6.65 \times 10^{-25}$ cm^{-2}), which makes a quasar difficult to detect.

3.2.2. NUMBER DENSITY The densities and radial locations of the absorbers are crucial for understanding their nature and origin. These two properties are tied together: determination of one yields the other via the ionization parameter (Equation 5). There are several ways to estimate the electron density (n_e), which is equivalent to determining the hydrogen density (n_H). The first relies on absorption lines from excited states that are populated by collisional excitation because the populations relative to the ground state depend on n_e and temperature (Osterbrock 1989). In the UV and far-UV, there are a number of fine-structure lines arising from just above ground level [e.g., Si II* λ1265, C II* λ1336, N III* λ992 (see Morton 1991)], as well as lines that arise from higher metastable levels in Fe II (Verner et al. 1999) and C III [i.e., the λ1175 multiplet (see Bromage et al. 1985, Kriss et al. 1992)]. Together, these lines probe a wide range of densities, $n_e \approx 10$–10^9 cm^{-3}, in low- to moderate-ionization gas. Densities have been determined in this way for NGC 4151, as described in Section 3.4, as well as several quasars (Hamann et al. 2001).

Another method for determining n_e is to make use of the absorption variability that is commonly observed. If it can be shown that the ionic columns have changed in response to a drop in the ionizing continuum, for example, then the time delay can be equated to the recombination time, which is inversely proportional to n_e. A proper evaluation of the recombination time for an ion X_i takes into account the recombinations of X_{i+1} to X_i and X_i to X_{i-1} (e.g., Krolik & Kriss 1995, Bottorff et al. 2000):

$$t(X_i) = \left[\alpha(X_i) n_e \left(\frac{f(X_{i+1})}{f(X_i)} - \frac{\alpha(X_{i-1})}{\alpha(X_i)}\right)\right]^{-1}, \quad (7)$$

where $\alpha(X_i)$ is the recombination coefficient for ion X_i and $f(X_i)$ is the fraction of element X in ionization state i. Nearly all of the absorption variations that have been detected have resulted from "snapshots" at two or more epochs, rather than intensive monitoring. These have resulted in upper limits on $t(X_i)$, lower limits on n_e, and hence upper limits on the radial location (see Section 3.2.3).

NGC 3516 currently provides the tightest constraints on the high-column X-ray absorber. Netzer et al. (2002) interpreted variations in the X-ray absorber at low energies over ~60 ks as primarily changes in the O VI opacity. Using this as an upper limit to the O VI recombination time gives $n_e > 2 \times 10^6$ cm^{-3}. By identifying the high-column, low-velocity UV absorbers in NGC 3516 with the X-ray absorber, Kraemer et al. (2002) find that the absence of C III* λ1175 absorption yields $n_e < 10^9$ cm^{-3}.

For the emission lines that presumably originate within the X-ray absorbers, the He-like triplets of O VII, Ne IX, and Mg XI provide density diagnostics. In particular, the ratio of the intercombination to forbidden line flux in the triplet provides n_e (Porquet & Dubau 2000) if the gas is photoionized (i.e., collisional ionization is not important). Thus far, only (rather large) upper limits have been obtained in this manner: Kaastra et al. (2002) find $n_e < 7 \times 10^{10}$ cm^{-3} for NGC 5548 and Kaspi et al. (2002) find $n_e < 10^{11}$ cm^{-3} for NGC 3783.

3.2.3. RADIAL LOCATION Clues on the relative location of an absorber can be obtained in several ways. Absorbers that cover the entire BELR, for example, must obviously lie at a greater distance r from the continuum source. In some cases, the absorber covers the entire NELR as well, indicating an origin in the host galaxy (Section 3.5). Rapid variability of the absorption columns and/or partial covering of the BELR would suggest a close proximity to the continuum source (although see the discussion regarding 3C 191 in Section 3.1.3). One method to determine r directly is to again make use of the absorption variability. If, for example, an absorption feature responds to an increase in the ionizing flux, the time lag can be associated with the ionization timescale (Krolik & Kriss 1997):

$$t_{ion} = \frac{h\nu_T}{F_{ion}\langle\sigma_{ion}\rangle}, \tag{8}$$

where $h\nu_T$ is the threshold ionization energy; $\langle\sigma_{ion}\rangle$ is the frequency-weighted photoionization cross section; and F_{ion} is the ionizing flux at the face of the cloud, such that $F_{ion} = L_{ion}/(4\pi r^2)$. A limit on r has been determined in this way for the component that is responsible for the C III* λ1175 absorption in NGC 4151: $r < 25$ pc (Espey et al. 1998); however, an actual value has been derived from n_e and U and is much smaller than this limit (Section 3.4).

Another method to determine r is from n_e, U, and the ionizing luminosity (Equation 5). For example, the limits on n_e mentioned above in the case of NGC 3516 give a distance of the UV/X-ray absorbers from the continuum source in the range ~0.02–0.4 pc. Note that the relative thickness of an absorber in the radial direction is given by $\Delta r/r$, where $\Delta r = N_H/n_H$. Given a typical column density of $N \approx 2 \times 10^{21}$ cm^{-2} for a single low-velocity component in NGC 3516 (Kraemer et al. 2002), the relative thickness of a typical absorber is in the range 4×10^{-5} to 8×10^{-4}, which indicates very "thin" absorbers in the radial direction, rather than a continuous wind.

3.2.4. MASS AND MASS-LOSS RATE The mass of an absorber, assuming spherical outflow, is given by $M_{abs} = 4\pi r^2 N_H m_p C_g$, and the mass loss rate is $\dot{M}_{abs} = M_{abs}/t_c$, where $t_c = r/v_r$ is the radial travel time. For NGC 3516, taking the total column density of $N_H = 7.7 \times 10^{21}$ cm^{-2} from the photoionization models (summed over all components), and assuming $C_g = 1$ gives $M_{abs} = 118\ M_\odot$. This is significantly larger than the mass of the ionized gas in the BELR, which based on the Hβ luminosity of NGC 3516 is $\sim$1 $M_\odot$ (Peterson 1997, but see Baldwin et al. 2002). Adopting an average radial velocity of $v_r = -200$ km s^{-1} for the UV absorbers, the lower limit to n_e, and assuming purely radial motion, the crossing time is $\sim$1900 years and the mass outflow rate is $\dot{M}_{abs} = 0.06\ M_\odot$ year^{-1}. Adopting the upper limit to n_e yields $t_c = 85$ year and $\dot{M}_{abs} = 0.003\ M_\odot$ year^{-1}. Thus, the mass outflow rate from the inner regions of NGC 3516 is in the range 0.003–0.06 $M_\odot$ year^{-1}, which is comparable to the mass accretion rate of 0.01 $M_\odot$ year^{-1} based on the bolometric luminosity of NGC 3516 ($\sim 10^{44}$ ergs s^{-1}) and an expected efficiency of $\sim$0.1 in the conversion of mass infall to energy (Peterson 1997).

3.3. The Importance of Variability

Variability may hold the key to understanding the intrinsic absorbers in AGN because it is the only way in many cases to determine the parameters described above. Variable absorption was first detected in optical spectra of NGC 4151 (Section 1.2), and subsequent IUE studies found that a number of AGN show absorption lines that vary in equivalent width (Crenshaw et al. 1999, and references therein). Variability has also been detected in a number of X-ray warm absorbers (George et al. 1998c, and references therein), dating back to their discovery (Section 1.2.2). To date, all of the variations have been consistent with changes in the ionic column densities and not the radial velocities. In the past, variations in the column densities have been attributed to (*a*) changes in the ionization of the gas, due to variations in the ionizing continuum, or (*b*) changes in the total column density (i.e., N_H), due, for example, to bulk motion of gas across the line of sight. It is now clear that both sources of variability are at work, sometimes in a single object, e.g., NGC 4151 (Kraemer et al. 2001b), and that multiple observations at high spectral resolution are required to distinguish between these sources and to identify the timescales over which they operate. In the UV, only four Seyfert 1 galaxies (NGC 3516, NGC 3783, NGC 4151, and NGC 5548) have been observed more than once at high spectral resolution, and each has shown variable ionic columns in one or more of the kinematic components (Kraemer et al. 2001a,b, 2002; Crenshaw et al. 2003).

The most dramatic case of variable ionization of the UV absorbers is provided by NGC 4151 (Crenshaw et al. 2000b, Kraemer et al. 2001b) in which a decrease in the UV continuum flux by a factor of $\sim$4 over two years coincided with a huge increase in the strengths of the low-ionization absorption lines. This is demonstrated in Figure 6, which shows the region around the peak of the C IV emission line. The low-state spectrum shows broad Si II (resonance and fine-structure) and metastable Fe II absorption lines, which are clearly not present in the high-state spectrum.

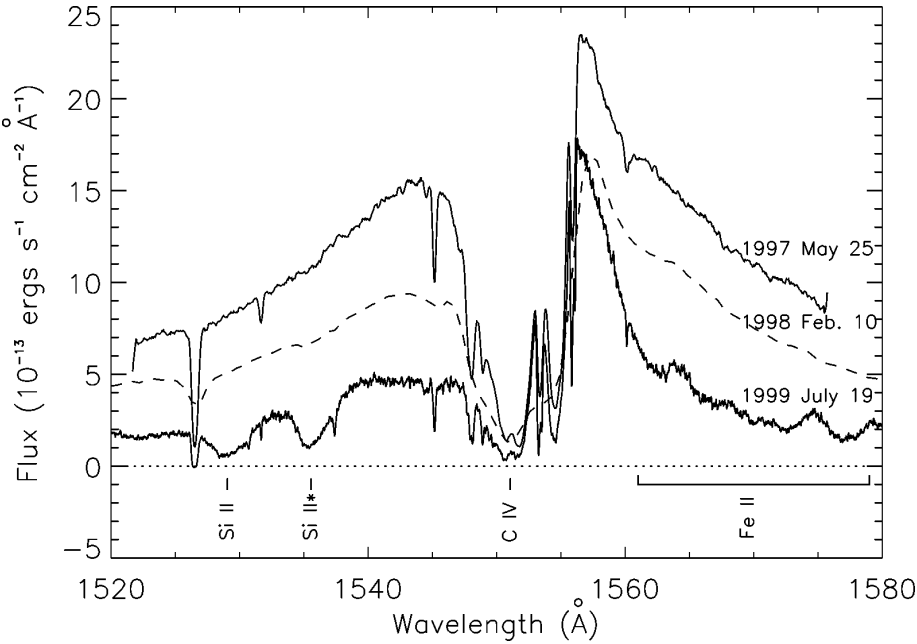

Figure 6 STIS spectra of the nucleus of NGC 4151 in the C IV region. A low-resolution spectrum from 1998 is plotted as a dashed line; the other two spectra are from echelle observations. Prominent broad absorption lines are labeled in the bottom (low-state) spectrum.

The broad variable absorption is from component "D + E" in Weymann et al. (1997) at a radial velocity of -490 km s^{-1} (relative to systemic); the metastable C III absorption also comes from this component, indicating a density of $n_H \approx 3 \times 10^9$ cm^{-3}, consistent with a rapid response of the absorption to the ionizing continuum (Kraemer et al. 2001b). Most of the absorption lines in component D + E are completely saturated, and yet they do not reach zero flux in their troughs due to scattered light from the nucleus. This arises in a region that extends outside of D + E as projected onto the sky. The comparitively high column density of this component ($N_H = 2.75 \times 10^{21}$ cm^{-2}) and the scattered light (~15% of the high state) in the troughs is reminiscent of low-ionization BAL quasars (Sprayberry & Foltz 1992), although the velocities and columns are not as high in NGC 4151. Given N_H and U from a photoionization model, the distance of D + E from the continuum source is only ~0.03 pc (Kraemer et al. 2001b).

The absorption variability (or lack thereof) of the other components of absorption in NGC 4151 permits tight constraints on U and N_H, given the requirement that photoionization models must match the ionic columns at both low and high states. Furthermore, the densities of these components are constrained by the low-ionization fine-structure lines. Thus, the absorbers in NGC 4151 have been mapped in unprecedented detail, revealing a huge range in distances ($r = 0.03$–2150 pc),

number densities ($n_H = 10^1 - 3 \times 10^9$ cm^{-3}), and columns ($N_H = 1.0 \times 10^{18} - 2.75 \times 10^{21}$ cm^{-2}). Both number and column densities decrease uniformly with distance, but there are no other obvious correlations [such as radial velocity with distance (see Kraemer et al. 2001b)]. However, none of the UV absorbers have been linked to the high ionization, high column X-ray absorber [$U = 0.9$, $N_H = 4 \times 10^{22}$ cm^{-2} (see George et al. 1998c, and references therein)].

If radiation pressure is driving the clouds outward, one might expect that component D + E would show a significant radial acceleration due to its proximity to the continuum source. However, no change in radial velocity has been detected for any component over seven years of monitoring (Weymann et al. 1997, Kraemer et al. 2001b). One possible explanation is that component D + E is too optically thick for efficient radiative acceleration. Another possibility is that the gas has a significant component of transverse motion (for example, accelerating in a "flow tube" at some angle to the line of sight; see Section 4), but the portion that is seen in absorption against the background emission is always at the same radial velocity.

Perhaps the strongest case for bulk motion as a source of absorption variability is given by NGC 3783, as demonstrated by HST spectra of the C IV region in Figure 7

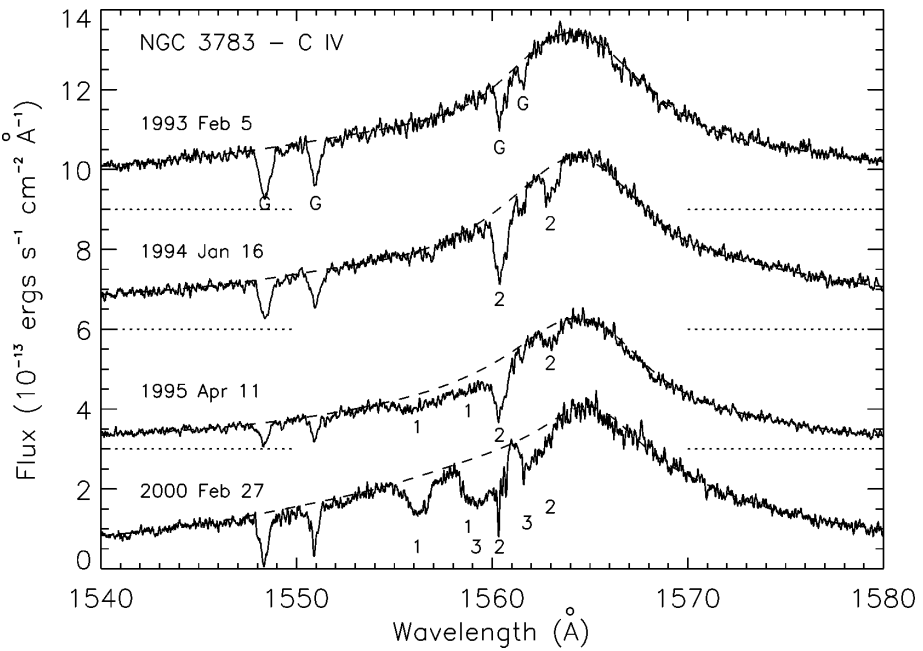

Figure 7 GHRS (*top three plots*) and STIS spectra (*bottom plot*) of the C IV region in NGC 3783. The zero flux levels are given by dotted lines. Galactic absorption lines (from C IV and C I) are indicated with a G, and the three kinematic components of the intrinsic C IV doublet are numbered.

(Kraemer et al. 2001a). Only Galactic absorption features were present in February 1993, but a C IV doublet (component 2) appeared 11 months later at a radial velocity of -550 km s^{-1}. Another component (component 1) appeared after a subsequent 15 months at -1370 km s^{-1}. In the final spectrum, obtained $\sim$5 years later, component 1 was much stronger, and component 2 was weaker; meanwhile, a new broad component (component 3) appeared at a radial velocity of -720 km s^{-1}. Clearly, the absorption variations are undersampled, but it is interesting that the continuum levels are all nearly the same, except for the lower level in 1995. The appearance and disappearance of absorption components appears to be independent of continuum flux (see Kraemer et al. 2001a for more details), which indicates transverse motion across the BELR on a timescale of one year. It is important to note that monitoring observations such as these are the only way to obtain transverse velocities. Recent evidence, from the only intensive UV monitoring campaign on a Seyfert 1 galaxy at high spectral resolution (Gabel et al. 2003), indicates that variable ionization is also important in NGC 3783 on shorter timescales of days to weeks.

3.4. The Connection Between UV and X-Ray Absorbers

The notion that the UV and X-ray absorbers originate in the same gas, characterized by a single ionization parameter (Section 1.2.3), is now clearly obsolete. As discussed in previous sections, the individual kinematic components in the UV show a wide range in ionization, and most produce negligible O VII or O VIII absorption in the X-ray region. Furthermore, the X-ray absorber itself is often complex and composed of at least two zones with different ionization parameters (e.g., Morales et al. 2000; Krolik & Kriss 2001, and references therein). Nevertheless, many X-ray absorbers have sufficiently high total column densities to produce observable ($\gtrsim 10^{13}$ cm^{-2}) ionic columns for UV absorption lines like N V and C IV, even though these represent trace ions in the gas. If a connection can be made, the UV component provides valuable kinematic information on the X-ray absorber that cannot be obtained with the current generation of X-ray telescopes. Because the absorbers can be extremely variable, simultaneous UV, far-UV, and X-ray observations at high spectral resolution are important for investigating this connection. These have recently become available.

NGC 3516 and NGC 3783 provide the strongest cases to date for UV components of absorption that arise from an X-ray absorber. In NGC 3516 (Section 3.2), photoionization models indicate that the low-velocity, high-column UV absorbers can provide all of the observed X-ray absorption (Netzer et al. 2002, Kraemer et al. 2002). In NGC 3783, several UV components provide the observed O VII column, but only a small fraction of the O VIII column (Kraemer et al. 2001b), confirming evidence for at least two components of X-ray absorption (George et al. 1998b). However, most of the UV counterparts to X-ray absorbers have yet to be clearly identified; in most cases, this is probably due to blending with absorption lines from lower-ionization components (cf., Kraemer et al. 2003).

Although most UV and X-ray absorbers do not arise from the same gas, there is a statistical connection that indicates a physical and/or geometric relationship between the two. Crenshaw et al. (1999) found that there is a one-to-one correspondence between Seyfert 1 galaxies that show intrinsic UV absorption and those that show intrinsic X-ray absorption. Kriss (2002) found the same connection between far-UV (O VI) and X-ray absorbers. Finally, Brandt et al. (2000) found that in a sample of quasars at $z < 0.5$, the equivalent width of the C IV absorption increases as the ratio of the optical to X-ray luminosities increases. Because the latter may be due to increasing absorption at $\sim$2 keV, this relation suggests a direct correlation between the strengths of the UV and X-ray absorption. The BAL quasars are at the extreme end of this relationship, at large EW (C IV) and weak X-ray flux. Several studies have concluded that the weak X-ray fluxes (including X-ray nondetections) of BAL quasars in general are due to X-ray absorption, rather than intrinsically weak fluxes (Gallagher et al. 2002; Green et al. 2002, and references therein).

Recent simultaneous observations have provided an intruiging clue to the connection between UV and X-ray absorbers. For AGN with the highest quality observations, the velocity coverage of the UV and X-ray absorbers is strikingly similar. Figure 8 shows a comparison of profiles (as a function of radial velocity, relative to the host galaxy) from the UV and X-ray observations of NGC 5548 (Crenshaw

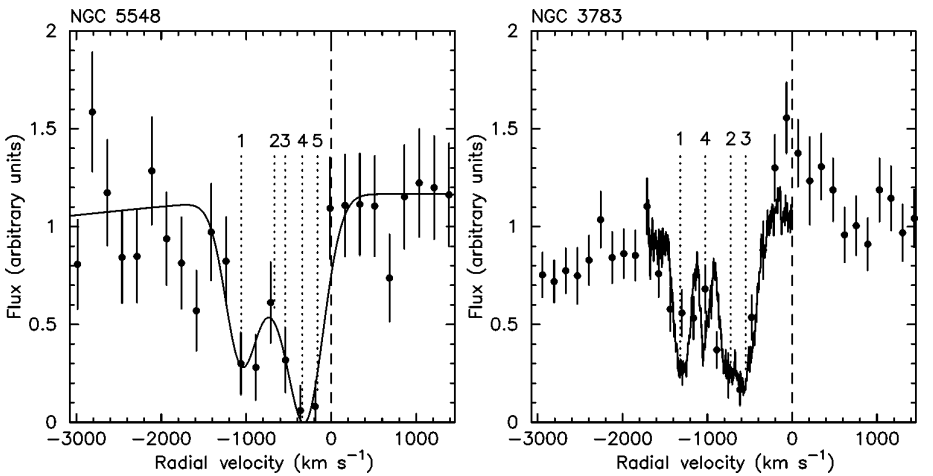

Figure 8 The velocity profiles of the C VI λ33.736 (*left*), and O VII λ21.602 (*right*) absorption lines from the CXO/LEG spectrum of NGC 5548 and CXO/MEG + HEG spectrum of NGC 3783 (adapted from Kaastra et al. 2002 and Gabel et al. 2003, respectively). The vertical dotted lines indicate the separate kinematic components identified in the UV. The solid curves show the model obtained by fitting the five kinematic components (see also Figure 1) in the case of NGC 5548, and the observed H I Lyβ profile in the case of NGC 3783. O VII λ21.602 emission at the systemic velocity is apparent in the case of NGC 3783 (see Kaastra et al. 2002, Kaspi et al. 2002, and Gabel et al. 2003 for details).

et al. 1999, Kaastra et al. 2002) and NGC 3783 (Kaspi et al. 2002, Gabel et al. 2003). Despite the relatively low resolution of the CXO X-ray spectra, it can be seen that there are clearly two components of X-ray absorption that appear to match the UV components 1 and 2–5 in NGC 5548, and 1–4 and 2–3 in NGC 3783. These observations suggest that the UV and X-ray absorbers share the same velocity field and are therefore possibly located in the same vicinity. One possible interpretation is that the UV components arise from high-density knots in an outflowing X-ray wind (Krolik & Kriss 1995, 2001).

3.5. Dust in the Absorbers

Determining if there is dust in the absorbers is important because it (*a*) provides clues to their origins, (*b*) affects the elemental abundances in the gas phase and therefore the ionic columns used for photoionization models, and (*c*) is important for radiative acceleration models (Section 4). X-ray observations of several reddened Seyfert 1 galaxies have shown that N_{HI} is much smaller than the total column (N_H) derived from the reddening (Komossa 1999, and references therein). Thus, it has been suggested that the reddening comes from a "dusty warm absorber" (Brandt et al. 1996, Reynolds 1997, Komossa & Bade 1998) in which nearly all of the H is ionized. However, Kraemer et al. (2000b) found that dusty "lukewarm absorbers," characterized by strong, and in some cases saturated, UV absorption lines (C IV, N V, Si IV, and Mg II), would be a better alternative because they can be placed at sufficient radial distances ($\gtrsim$100 pc) to explain the observed reddening of the NELRs in these AGN. These absorbers were subsequently identified in HST spectra of the reddened Seyfert 1 galaxy NGC 3227 (Crenshaw et al. 2001) and the narrow-line Seyfert 1 galaxy Akn 564 (Crenshaw et al. 2002b). In both cases, photoionization models of the UV absorption lines confirmed that the columns of gas ($N_H = 1\text{–}2 \times 10^{21}$ cm^{-2}) were sufficient to provide the observed reddenings, assuming a dust-to-gas ratio similar to the Galactic value given by $N(H) = 5.2 \times 10^{21} E(B-V)$ cm^{-2} (Shull & van Steenberg 1985).

Crenshaw et al. (2001, 2002b) suggested that the dusty lukewarm absorbers in NGC 3227 and Akn 564 lie in the galactic disks of their host galaxies because (*a*) the host galaxies are both inclined by $\sim 60^\circ$, so that our line of sight intercepts more gas and dust than for face-on galaxies, (*b*) their radial velocities are within 200 km s^{-1} of the systemic velocities, and (*c*) the depths of the UV lines confirm that the absorbers cover their NELR. A subsequent study of a large sample of Seyfert 1 galaxies confirmed this suggestion (Crenshaw & Kraemer 2001). There is a general trend of increasing UV color (i.e., increasing extinction) with increasing inclination angle of the host galaxy, and all of the reddened, inclined Seyfert 1 galaxies observed at $R \geq 1000$ show evidence for dusty lukewarm absorbers. Thus, these dusty absorbers lie (and possibly originate) in the disks of the host galaxies.

For the UV and X-ray absorbers that are thought to be intrinsic to the nucleus, there is evidence that some contain dust and some do not. Most of the detected

X-ray absorbers do not contain significant amounts of dust because their columns ($N_H = 10^{21}$–10^{23} cm^{-2}) imply reddening values of E(B−V) = 0.2–20, which in most cases are much larger than observed. This would suggest that these X-ray absorbers are inside, or originated inside, the dust sublimation radius, which is ∼0.13 pc for a typical Seyfert 1 galaxy with a UV to X-ray continuum luminosity of 10^{44} ergs s^{-1} (see Section 4.2). However, the possibility remains that a small fraction of warm absorbers are dusty [e.g., MCG-5-30-15 (Lee et al. 2001)]. Such a suggestion remains both controversial and crucial in the interpretation of the soft X-ray spectra of AGN (Lee et al. 2001, Sako et al. 2003).

The column densities of most outflowing UV absorbers are too small for direct detection of dust by reddening. The two Seyfert 1 galaxies with sufficiently high UV columns ($N_H \approx 3 \times 10^{21}$ cm^{-2}), NGC 4151 and NGC 3516, do not show associated reddening, which is consistent with other evidence that these absorbers are located inside the dust sublimation radius (Kraemer et al. 2001b, 2002). On the other hand, there is indirect evidence, via depletion of carbon, that the outflowing absorbers in NGC 5548 may contain dust (Crenshaw et al. 2003), although another possibility is that carbon is depleted and nitrogen is enhanced through the CNO process in intermediate-mass stars (Maeder & Meynet 1989). In quasars, there is statistical evidence for dust in the UV absorbers; quasars with narrow absorption lines have systematically redder continua (Baker et al. 2002, Vestergaard 2003), and BAL quasars tend to be redder than normal quasars (Brotherton et al. 2002). Further studies of dust in the absorbers are needed to probe their origins. Dust-free absorbers likely reside or originate within the dust sublimation radius, whereas absorbers with dust either originated outside of this radius or have picked up dust along the way [e.g., from the putative torus (Krolik & Kriss 1995)].

3.6. Correlation Analyses

Statistical correlations between the properties of absorbers and other AGN properties (e.g., luminosity, radio power, mass, relative accretion rate, orientation with respect to the line of sight) have the potential to provide important constraints on dynamical models. Most of the work in this area has concentrated on UV absorption because high-quality X-ray observations of AGN are rather limited at present, and on quasars (in some cases combined with Seyferts), because the Seyfert 1 sample alone is limited to a relatively small range in redshift and luminosity. As discussed in Section 3.1.5, narrow (FWHM < 500 km s^{-1}) UV absorption is probably equally common in both low-redshift, moderate-luminosity Seyferts and high-redshift, high-luminosity quasars. However, BALs and high-velocity narrow lines only occur in quasars. Intrinsic absorption may be rare in low-luminosity AGN, but more observations are needed to confirm this and to determine if luminosity or some other property is the controlling factor.

Statistical studies using well-defined samples have recently become available. Laor & Brandt (2002) find that in $z < 0.5$ quasars and Seyferts, the C IV *EW* and maximum radial velocity increase with increasing ultraviolet luminosity, which

is expected for outflow driven by radiation pressure. Vestergaard (2003) finds a similar correlation between *EW* (C IV) and luminosity in a higher redshift ($1.5 < z < 3.5$) sample. In terms of radio power, Vestergaard finds that roughly equal percentages ($\sim$50%) of radio-loud and radio-quiet quasars show narrow UV absorption lines. However, lobe-dominated quasars, presumably viewed with the jets near the plane of the sky, appear to have more frequent and stronger absorption than core-dominated radio quasars. This may indicate higher column densities in the equatorial regions (defined by the accretion disk), consistent with predictions of disk-wind models (Section 4). Vestergaard suggests that the strong equatorial flows in radio-loud quasars may be analogs to BALs found in radio-loud and radio moderate quasars. For radio-quiet AGN, including Seyferts, reliable indicators of orientation (i.e., inclination of accretion disk) with respect to the line of sight are needed; possible indicators are H_2O masers (Gallimore et al. 1996, Greenhill et al. 1996), Fe Kα profiles (Nandra et al. 1997, Turner et al. 1998), and kinematic models of the NELR (Crenshaw et al. 2000a, Ruiz et al. 2001). Obviously, more studies are needed to test the above correlations and to explore their significance.

4. DYNAMICAL MODELS

Models that attempt to explain the origin and means of acceleration of mass outflow in AGN must address the following properties: the effects of the luminosity of the central engine, the circumnuclear distribution of the gas, the lack of evidence for radial acceleration, the evidence for transverse motion, and the range in ionization states (hence, density?) among subcomponents at the same radial velocities. Elvis (2000) proposed a model for the structure of quasars that unifies all the emission, absorption, and reflection phenomenology of AGN in the form of a flow of warm gas from the accretion disk. Although this geometric approach is helpful in exploring empirical connections between AGN components, it does not address the underlying physics of the outflow phenomenon. In the following subsections, the most popular physical models of the dynamics of mass ouflow are reviewed.

4.1. Compton Heated Winds

A possible source of outflow is in the form of a thermal wind arising from the putative accretion disk (Begelman et al. 1983). In this scenario, the EUV and X-ray radiation emitted from the region near the central black hole irradiates the surface of the accretion disk at large radii. Because the disk itself is optically thick to the radiation, in order for the outer parts of the disk to be irradiated, either the height of the disk must increase faster than $1/R$ (see Shakura & Sunyaev 1973), the central continuum source must lie above the disk, or the X-ray radiation must be scattered onto the surface of the disk. In gas of density $n_H \leq 10^{12}$ cm^{-3}, for $T \leq 10^5$ K, ionization heating is balanced by line cooling and recombination. If

the ionization parameter is sufficiently high, line cooling is suppressed, and the gas reaches a hot phase in which Compton heating of the gas is balanced by cooling via the inverse Compton process, with an equilibrium temperature close to its Compton temperature such that, $kT_{IC} = 1/4\,\langle\epsilon\rangle$, where the average photon energy $\langle\epsilon\rangle = L^{-1}\int_0^\infty h\nu L_\nu\, d\nu$, and L is the luminosity of the central source. Also, there is a region of intermediate temperature over which the gas is thermally unstable or, more likely, marginally stable (Krolik & Kriss 2001), although the exact nature of a multiphased photoionized gas depends on the SED of the ionizing continuum (see Section 2.3.1). An accretion disk is thin if the local sound speed at a particular radius is very much less than the Keplerian speed (Shakura & Sunyaev 1973), and the vertical scale height of the disk is related to its radial distance through the ratio of these two parameters. At large vertical distances, the pressure and density of the disk drop, and the gas can reach the Compton heated phase. If the isothermal sound speed in the gas is less than the escape velocity, which is a function of black hole mass (M) and radial distance (R_0), the hot phase will form a hydrostatic corona above the disk's photosphere. One may define an "escape temperature," $T_g = GM\mu/R_0k$, where μ is the mass of a hydrogen atom. If the sound speed exceeds the escape velocity, or $T_{IC}/T_g > 1$, a thermal wind will arise. Because the Compton temperature, and hence the sound speed, is a function of the SED of the ionizing radiation rather than its intensity, while the escape velocity decreases with radius, winds are possible at radii greater than $R = GM\mu/kT_{IC}$. In the region where winds can form, the gas arising from the disk may not have had time to reach its Compton temperature before reaching a distance R_0. Hence, one can define a "characteristic temperature," $kT_{ch} = \Lambda_0(R_0/c_{ch})$, where Λ_0 is the optically thin heating rate evaluated at R_0 and c_{ch} is the sound speed at T_{ch}. The condition where T_{IC}, T_g, and T_{ch} are all equal defines a critical luminosity, $L_{cr} = 0.03\,(T_{IC8})^{-1/2}L_E$, where $T_{IC8} = T_{IC}/10^8$ K and L_E is the Eddington luminosity. The ratio L/L_{cr} characterizes the wind's effectiveness in overcoming gravity. Notably, this depends only on the Compton heating, rather than radiation pressure.

The discovery of polarized nuclear continuum emission in Seyfert 2 galaxies (Miller & Antonucci 1983) and the suggestion that the continuum source of the radiation in the BELR in these galaxies is hidden by dense molecular tori led to a model linking the Compton heated winds and the warm reflecting gas (Krolik & Begelman 1986, 1988). In this model, however, the source of the wind is the molecular torus, rather than the accretion disk. If the luminosity of the central source is $\geq 0.08L_E$, the flow can overcome the central gravitational potential and a substantial wind will form (Balsara & Krolik 1993), reaching a temperature of $\sim 1 \times 10^6$ K and flow speed of several hundred km s^{-1}. Following from this, Krolik & Kriss (1995) suggested the warm reflecting component was identical to the warm absorber detected in the X-rays. They argued that while the thermal wind may be the source of only some of the UV resonance line absorption from H I and Li-like species, other UV lines could form in lower ionization gas coexisting with the warm reflector/absorber, either as part of the two-phase medium described by Krolik et al. (1981) or dense, low ionization knots swept up by the outflowing

wind. In either case, a broad range of temperature and ionization can exist in the flow (Krolik & Kriss 1995, 2001) and the UV and X-ray absorbers could then be dynamically linked.

4.2. Radiatively Driven Flows

Radiation pressure is an attractive means for accelerating gas from an AGN, if only for the reason that the central engine is a tremendous source of continuum radiation (most of the work on radiative acceleration has been done for BAL quasars, but it is also applicable to the outflow in Seyfert galaxies). The radial equation of motion for material under the influence of radiation pressure and gravity at a distance r from a central point mass M can be written as:

$$v\frac{dv}{dr} = \frac{\kappa L}{4\pi r^2 c} - \frac{GM}{r^2}, \tag{9}$$

where v is the velocity of the accelerated gas, κ is the absorption cross-section per unit mass (the exact nature of which depends on the source of opacity to the radiation), L is the luminosity of the central source, and c is the speed of light. As shown below, the ability to drive sub-Eddington flows depends on κ, which in turn depends on the velocity structure and the optical depth in the accelerated gas. Further, the asymptotic terminal velocity can be expressed as:

$$v_\infty = \left[\frac{2}{r_0}\left(\frac{\kappa L}{4\pi c} - GM\right)\right]^{1/2}, \tag{10}$$

where r_0 is the radial launch point of the gas.

The dynamics of dusty, radiation-driven gas in the context of mass flow from within the BELR of AGN has been discussed extensively. Scoville & Norman (1995) suggested that quasar BALs originate in stellar contrails, formed when dusty gas supplied by circumstellar mass loss from evolved stars is exposed to the UV continuum radiation from the central source. Another possible source for dusty gas is the accretion disk. Radiative driving of embedded dust may give rise to radial acceleration of magnetohydrodynamic (MHD) flows (Königl & Kartje 1994) or may provide a means of elevating gas from the disk (Emmering, et al. 1992) (these models are discussed in more detail in the following subsections). Dusty gas has a high effective opacity; e.g., depending on the spectral energy distribution of the continuum radiation, the dust/gas ratio, and grain-size distribution (e.g., Mathis et al. 1977), the ratio of the flux-weighted dust opacity to the Thomson opacity is $\approx 5 \times 10^2$–10^3. In regions where the dust is optically thin and dynamically well-coupled to the gas, the radiation pressure force on the dust plus gas can easily exceed the gravitational force, even for highly sub-Eddington luminosities (e.g., Phinney 1989, Pier & Krolik 1992, Laor & Draine 1993). Requiring that the gas and dust are well-coupled is equivalent to assuming that the radiation pressure force on the grains is roughly equivalent to the gas-grain collisional drag force. In an intense radiation field, the grains are likely to become highly positively charged

(see Scoville & Norman 1995). In this case, the grains will become coupled to the gas via the embedded magnetic field.

Although radiative acceleration may be important for dusty gas, grains cannot exist in unshielded gas in close proximity to the central source, as the continuum radiation will heat the grains to their sublimation temperatures. The minimum distance where grains can exist is $r_{min} \approx 1.3\, L_{46}^{1/2} T_{1500}^{-2.8}$ pc, where L_{46} is the UV luminosity of the central source in units of 10^{46} ergs s^{-1} and T_{1500} is the sublimation temperature of the grain in units of 1500 K (Barvainis 1987). Note that the dust can exist much closer to the central source if the UV radiation has been attenuated (e.g., Emmering et al. 1992).

At distances $< r_{min}$, the gas will be dust-free, but may still be radiatively accelerated via bound-bound (i.e., "line driving") and bound-free transitions within the irradiated gas (the cross section for Compton scattering is relatively quite small). In their models for line-driven winds in hot stars, Castor et al. (1975) demonstrated that the most efficient mechanism for extracting momentum from the radiation field and driving a powerful outflow is via line opacity. Following Castor et al., one can parameterize the efficiency of line driving in terms of the ratio of line scattering to electron scattering:

$$\eta = \frac{\pi e^2}{m_e c} g f \frac{n_L/g_L - n_U/g_U}{n_e \sigma_{\rm T} \Delta\nu_{\rm Dop}}, \tag{11}$$

where e and m_e are, respectively, the charge and mass of the electron; g is the statistical weight of the state; f is the oscillator strength of the line; n_L, n_U and g_L and g_U are, respectively, the number densities and degeneracies of the lower and upper states; n_e is the electron density, $\sigma_{\rm T}$ is the Thomson cross-section; and $\Delta\nu_{\rm Dop} = \nu_{\rm line} v_{\rm Th}/c$ is the Doppler width of the line, where $\nu_{\rm line}$ and $v_{\rm Th}$ are the frequency and thermal width of the line, respectively. For resonance lines, the upper level can be neglected. The equivalent electron optical depth scale is $t = \sigma_{\rm T} \epsilon n_e v_{\rm th} (dv/dr)^{-1}$, where $v_{\rm th}/(dv/dr)$ is the electron optical depth of a Sobolev length and the factor ϵ depends on the volume filling factor of the accelerated gas (ϵ is $\ll 1$ for small, dense clouds). Hence, the optical depth of a line at any point is simply $\tau_{\rm line} = \eta t$. Further, the ratio of the line acceleration to the acceleration due to Thomson scattering, or "force multiplier," is

$$M_L(U,t) \equiv \frac{1}{F} \sum_l F_{\rm line} \Delta\nu_{Dop} \frac{1 - e^{-\eta t}}{t}, \tag{12}$$

where U is the ionization parameter (see Section 2.3.1), F is the total flux, $F_{\rm line}$ is the continuum flux per unit frequency at the line, and the sum is over all of the resonance lines. The dependence on U arises implicity via η in that, because efficient line driving requires the presence of bound electrons, η will approach zero as the gas becomes highly ionized. Hence, the force multiplier is a decreasing function of U as shown in Figure 9. The line contribution to the acceleration of the

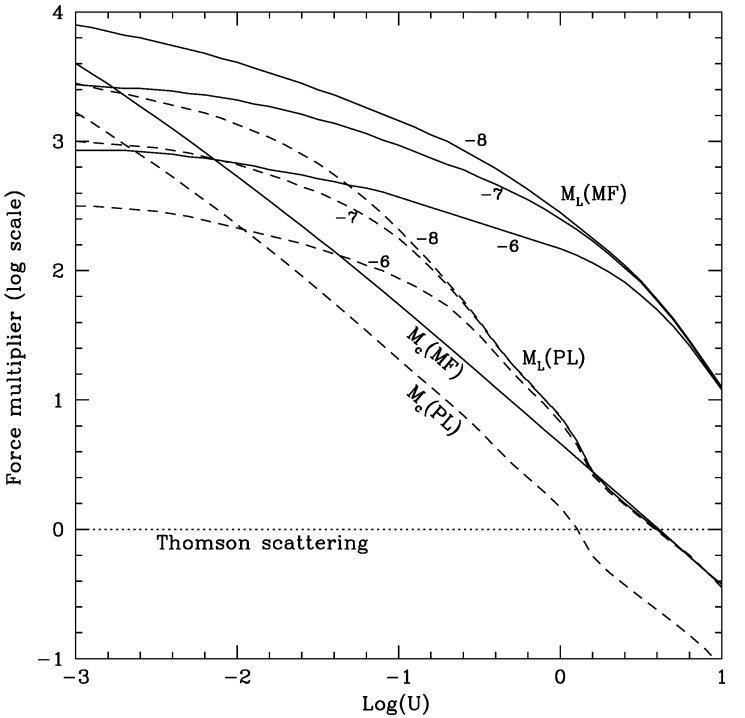

Figure 9 Force multipliers, M_L and M_c, as functions of U, for different ionizing continua (from Arav et al. 1994). MF stands for the Mathews & Ferland (1987) SED, and PL for a simple power-law SED, with $L_\nu \propto \nu^{-1}$. The three different curves are for different values of $\log(t) = -6, -7$, and -8.

gas is

$$a_{line} = \frac{n_e \sigma_T F}{\rho c} M_L(U, t), \tag{13}$$

where ρ is the mass density of the accelerated gas.

Bound-free transitions are additional sources of opacity for radiative acceleration, and hence one may also define a continuum force-multiplier (Arav et al. 1994, Chelouche & Netzer 2001):

$$M_c(U) \equiv \frac{\rho c}{n_e \sigma_T F} \int_0^\infty \frac{\kappa_\nu F_\nu}{\rho c}\, d\nu, \tag{14}$$

where κ_ν is the continuum opacity as a function of frequency. A smoothly accelerated flow will start out at a low velocity, pass through a sonic point, then through a critical point (see Castor et al. 1975, Abbott 1982), and finally asymptotically approach a terminal velocity. Mathematically, the critical point occurs where the sum of the inertial, gravitational, and pressure forces equal the driving force.

Arav & Li (1994) and Arav et al. (1994) modeled radiative acceleration of BAL clouds based on models of winds from hot stars (Castor et al. 1975). Given the assumption of small filling factors of the absorbing gas (Arav et al. 1994), cloud confinement is necessary. However, confinement by a hot ($\sim 10^8$ K) medium would require densities so large that radiative acceleration would be negligible [as it is in the thermal wind models described by Krolik & Begelman (1986)]. Hence, Arav et al. (1994) supposed that the confinement is nonthermal, e.g., via magnetic fields (see Rees 1987). They found that they could achieve high radial velocities and realistic absorption line profiles, including the drop in opacity toward higher velocities, if the BAL gas originated within $\sim$0.1 pc of the central source and was dynamically coupled to a hot confining medium. If the clouds are indeed coupled to a more highly ionized medium, such as the Compton-heated wind, the friction between the clouds and the medium is so large that the system responds as a single fluid. In this case, the flow can be driven supersonically by resonance-line acceleration of the entrained clouds. The efficiency of this process is highest when the product of the line opacity and the ionization parameter is greatest, which in turn occurs when the clouds are irradiated by a soft ionizing continuum or one that has been modified by an intervening absorber that is optically thick at the He II bound-free edge. The model line profiles produced by this model are smooth and featureless, unlike those observed, which suggests the possibility of the superposition of absorbers with different velocities and/or the presence of a nonradial component.

Chelouche & Netzer (2001) examined the dynamics of the high ionization gas detected as "warm" absorbers in many AGN. They assumed the absorbers to be in rough hydrostatic equilibrium at all locations and to be magnetically confined. Although the bound-bound cross-sections are the largest in dust-free gas, in their models there are no changes in density or velocity across the clouds; thus, line saturation and self-shielding will restrict the contribution of line driving to the surface layers. In absorber clouds with column densities $N_H > 10^{21}$ cm^{-2} and $U \approx 1$, typical of "warm absorbers" (Reynolds 1997, George et al. 1998c), bound-free transitions will dominate the radiative acceleration.

Murray et al. (1995) (see also Murray & Chiang 1995) considered a model in which broad absorption lines form in a radiatively driven accretion disk wind. Contrary to previous work, Murray et al. modeled the absorbers as part of a continuous outflow rather than individual clouds. The wind originates over a range of radial points along the disk. The vertical acceleration of the wind from the disk is due to line driving by UV photons emitted from the disk directly below the wind, whereas the radial acceleration is due to the UV photons emitted from the central regions of the disk. Because the wind is constantly replenished from the disk, there is no need for external confinement, and the density of the wind decreases with increasing distance. As noted above, line driving will cease if the gas becomes overionized (one way to avoid this problem is to assume that the gas exists in dense clouds). Murray et al. calculated that this occurs when a wind exposed to an unattenuated soft X-ray flux achieves an ionization parameter $U \approx 60$. However, gas flow along

the innermost streamline creates pressure gradients that can accelerate neighboring gas. This so-called hitch-hiker gas can shield the wind from soft-X-rays; hence, the wind can remain in a low enough state of ionization to absorb UV photons. Because the ionization parameter of the hitch-hiker gas increases with velocity and distance, line driving will cease when the gas is some height, z, above the disk, and the gas will spiral back toward the disk. If z_c is the height of the critical point on a wind streamline, the wind can be further accelerated if $z_c \leq z$. The model predicts outflow velocities $\sim 0.1\ c$ and a very narrow (5°) opening angle for the wind, which is in general agreement with the properties of BAL quasars. However, in order to achieve high velocities, the inner edge of the wind must be at $r \approx 10^{16}$ cm for a $10^8\ M_\odot$ central mass, which is at least an order of magnitude smaller than a typical BELR. The hitch-hiker gas will have column densities $\sim 10^{23}$ cm^{-2}, which will produce strong X-ray absorption along the line of sight through the wind. Also, the models predict that the higher ionization UV lines, e.g., N V and C IV, will form closer to the central source than low ionization lines, such as Mg II, implying that these lines can only be observed when the source is viewed close to the disk, and the line of sight passes through many streamlines.

Proga et al. (2000) performed axisymmetric, time-dependent calculations of line-driven winds from accretion disks. An important result of these models is that a line-driven wind from the disk can survive without an external screen. As with the Murray et al. (1995) model, the winds are driven vertically by radiation from the disk and radially by radiation from the central source. The predicted gas streamlines are perpendicular to the disk over a height that increases with radius, but then bend away and become nearly radial. In the upper envelope of the wind, there is a large velocity shear between the fast-moving radial and lower density (hence highly ionized) gas moving inwards, as shown in Figure 10, which will give rise to Kelvin-Helmholtz instabilities. As the flow from the inner part of the disk is accelerated by line-force, its density decreases until it becomes overionized and falls back toward the disk. Because this component shields the gas at larger radii from the soft X-ray flux, there is no need to include a separate component such as the hitch-hiker gas suggested by Murray et al. Due to the instabilities in the wind, dense knots will be generated every few years. Hence, unlike the Murray et al. model, lower ionization lines can form within inner streamlines.

4.3. Hydromagnetic Flows

One mechanism for accelerating gas off an accretion disk is via an accretion-driven wind (see Rees 1987). The wind consists of ionized material in the disk corona that is frozen onto (locally) open, rotating magnetic field lines. As the field lines rotate, material is centrifugally accelerated above and away from the disk plane, akin to beads accelerated along a rotating wire. The field lines are anchored to the disk so mass ejected in the wind removes angular momentum from the disk and allows disk material to fuel the AGN engine. Coronal material is loaded onto magnetic lines from the disk via thermal expansion or magnetic bouyancy.

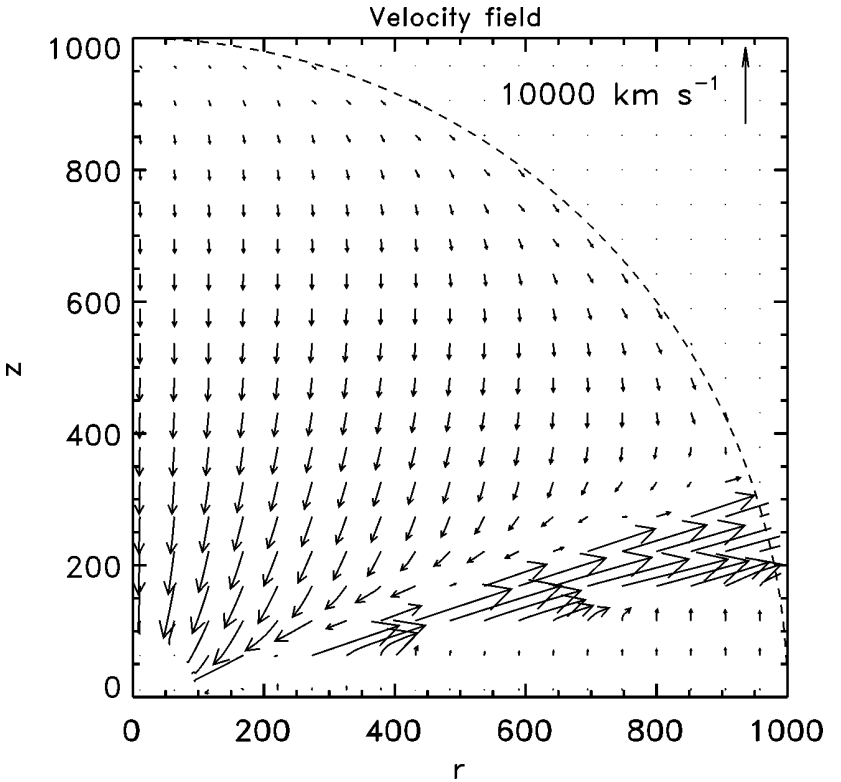

Figure 10 Map of the velocity field (poloidal component only) predicted by the disk-wind model of Proga et al. (2000). The rotation axis of the disk is along the left-hand vertical axis, whereas the midplane of the disk is along the horizontal axis.

Only some of the field lines will be favorably oriented for the acceleration of gas off the surface of the disk. Blandford & Payne (1982) illustrated the process by solving the MHD equations for a self-similar, axisymmetric, cold MHD flow from a Keplerian disk. In Newtonian hydrodynamics, self-similar solutions occur when (*a*) The spatial distribution physical quantities are functions of $x/l(t)$, where x and t are the spatial and time variables and $l(t)$ is a time-dependent scale function, and (*b*) all dimensional constants entering the initial and boundary conditions vanish or become infinite (Barenblatt & Zel'dovich 1972). Self-similar solutions therefore do not model the structure and generation of the magnetic field within the disk nor the reconnection of magnetic field lines far from the disk surface.

In steady state, the flow velocity can be described in terms of the magnetic field strength **B** and angular velocity ω by

$$\mathbf{v} = k\frac{\mathbf{B}}{4\pi\rho} + \omega \times \mathbf{r}, \tag{15}$$

where the second term on the right-hand side is simply the rotational velocity (see Chandrasekhar 1965, Mestel 1961). The quantity k can be considered as the ratio of constant mass flux over constant magnetic flux along a field line, as can be demonstrated from the mass continuity equation $\nabla \cdot (\rho \mathbf{v}) = 0$ (see Mestel 1961). For a self-similar flow, one assumes that $\rho \propto r^{-b}$ and $B \propto r^{-(b+1)/2}$ [note that the Alfven speed ($\propto B\rho^{-1/2}$) scales as the Keplerian velocity ($\propto r^{-1/2}$)]; Blandford & Payne (1982) assumed $b = 1.5$. Safier (1993a,b) noted that the density distribution above the disk is highly stratified as a consequence of the rapid acceleration of the gas as it is flung outwards, particularly at small angles with respect to the disk surface. In cylindrical coordinates (r, ϕ, z), with an origin at the center of mass of the black hole/disk system, the magnetic field lines have the form

$$\mathbf{R} = [\mathrm{r_o}\xi(\chi), \phi, \mathrm{r_o}\chi], \tag{16}$$

where r_o is the point where the field lines meet the surface of the accretion disk; χ is the coordinate along the field line; and $\xi(\chi)$ is chosen to satisfy the MHD flow equations subject to the scaling of ρ, B, and v_ϕ, with $\xi(0) = 0$. Similarly, the flow velocity is of the form

$$\mathbf{v} = [\xi'(\chi) f(\xi), g(\chi), f(\xi)] \left(\frac{GM}{r_0}\right)^{1/2}, \tag{17}$$

where prime denotes differentiation with respect to χ, f and g are chosen to satisfy the MHD flow equation (with $f(0) = 0$ and $g(0) = 1$), and M is the black hole mass. The function ξ' is of order unity at small χ, dropping as $1/\chi^{1/2}$ at large χ; hence, the flow is distinctly nonradial at large distances. The solution must satisfy the centrifugal ejection condition, which requires that the magnetic field lines at the base of the flow are inclined by $\theta \leq 60^\circ$ to the disk (Blandford & Payne 1982, Emmering et al. 1992).

Blandford & Payne (1982) suggested that this mechanism is responsible for the formation of relativistic jets as a result of the generation of a well-collimated, super-Alfvènic flow at large distances from the disk. The model was also applied to the formation and dynamics of BELR clouds by Emmering et al. (1992) and Bottorff et al. (1997). Emmering et al. suggested that dusty material is initially radiatively driven off the surface of the disk. As the gas is further exposed to the UV radiation from the central source, it becomes ionized and the dust grains may be destroyed, either due to sublimation or sputtering due to internal shocks. Subsequently, the photoionized clouds flow along the magnetic field lines embedded in the disk corona (see Figure 1 in Emmering et al. 1992). The clouds will expand at their sound speed ($s \approx 10$ km s^{-1}) until the gas pressure falls into rough equilibrium with that exerted by the ambient magnetic field ($\approx B^2/8\pi s^2$). The emission lines are broadened by both bulk motion and by electron-scattering of the line photons in the corona or disk.

Following Blandford & Payne (1982) and Emmering et al. (1992), Bottorff et al. (2000) applied the MHD flows to the dynamics of the intrinsic UV and X-ray

absorbers detected in Seyfert 1 galaxies. Similar to the BELR models (Emmering et al. 1992), the more highly ionized gas in which the X-ray absorption occurs lies at smaller radii, whereas the UV absorption lines form at larger distances. The nonradial nature of the flow provides a natural explanation for the changes in total column density reported in several Seyferts and the absence of evidence for radial acceleration of individual kinematic components (see Section 3.3).

4.4. Hybrid Models

Königl & Kartje (1994) adapted the approach of Blandford & Payne (1982), with additional refinements by Safier (1993a), in modeling MHD winds from accretion disks, with a set of solutions with $b = 1.0$–1.5, where b is the density decay exponent. They required that, subsequent to the magnetic acceleration off the disk, the wind is radiatively driven via the opacity of dust grains embedded within and dynamically coupled to the gas (similar to the initial acceleration of the clouds in the Emmering et al. model). They argue that such a wind can better explain the obscuration of the central regions of Seyfert 2 galaxies than a molecular torus, and the absorption and scattering of the ionizing continuum radiation by the wind can create the ionization cones seen in many Seyferts (e.g., Evans et al. 1991, Pogge & de Robertis 1993, Wilson et al. 1993). Königl & Kartje found that a value of $b = 1$ was necessary in order to confine the wind to the solid angle suggested by the fraction of Type 2 Seyferts (see Antonucci 1993). If the column density of the wind varies over time, as one might expect if the flow is not purely radial and the injection of mass into the flow is variable, this mechanism may help explain the variations in the X-ray absorber column densities reported in a number of Seyfert 2 galaxies (Risaliti et al. 2002).

De Kool & Begelman (1995) addressed the origin and confinement of radiatively driven clouds to explain the UV absorption in BAL quasars. Similar to the Emerring et al. (1992) model, the clouds form in a molecular accretion disk, threaded with magnetic field lines. However, the dynamical role of the magnetic field is quite different. The clouds are elevated from the disk, possibly by magnetic buoyancy, and are exposed to the ionizing radiation from the central source and heated to a warm ($T \approx 10^4$ K) thermal equilibrium. The magnetic field lines are dragged along with the elevated gas and prevent the heated clouds from expanding sideways. The clouds are subsequently radially accelerated, via resonance line driving, in a manner similar to that discussed by Arav & Li (1994) and Arav et al. (1994). The opening angle of the flow is set by equilibrium between the magnetic force and radiation force in the θ direction. The magnetic force per unit volume is the gradient of the magnetic pressure, or to order-of-magnitude, the magnetic pressure itself divided by the extent of the outflow in the θ direction, whereas the radiation force is proportional to the mass loss rate. If the magnetic field is responsible for the cloud confinement, the magnetic pressure must balance the gas pressure. Clouds emerging from the disk are accelerated nearly radially outwards, which compresses the magnetic field lines on which the gas is moving, up to a point where the magnetic forces become comparable to the radiation force. Thus,

when the radiation force is very strong, the flow is confined to a narrow wedge along the disk. The opening angle scales inversely with the radiation force and, hence, the mass loss rate. Assuming that the ionizing luminosity and accelerating luminosity are equal, a mass loss rate of 1 $M_\odot$ year^{-1} is required to provide a sufficient radiative force to compress the outflow to an opening angle of 0.1 rad. Such a mass loss rate is at the upper limit of that inferred from the UV absorption line profiles. A more acceptable mass loss rate of 0.1 $M_\odot$ year^{-1} could be achieved if the magnetic pressure, and hence the gas pressure, were a factor of ten less. De Kool & Begelman suggested that a column of highly ionized gas lying between the BAL clouds and the ionizing source could absorb ionizing radiation, hence reducing the gas pressure within the clouds without absorbing or scattering the UV flux, which does the line driving. They further suggested that the X-ray (warm) absorption may arise in the intervening gas. Note that the column density of the screening gas ($N_H \approx 10^{20}$–10^{22} cm^{-2}) is at least an order of magnitude smaller than that required of the inner edge of the wind in the models of Murray et al. (1995), and thus is consistent with the fact that several BAL quasars have normal optical to X-ray flux ratios (e.g., Green et al. 1995).

Recently, Proga (2003) studied the two-dimensional, time-dependent magnetohydrodynamics of radiation-driven disk winds. The radiation force is via resonance line driving. Although the initial conditions orient the magnetic field lines perpendicular to the disk due to the magneto-rotational instability and disk rotation, the toroidal field dominates the poloidal field above the disk. The gradient of the toroidal field drives a slow, dense outflow. Depending on the relative strengths of the magetic field and the system (disk + central source) luminosity, the wind can be primarily radiation- or MHD-driven. The former predicts a slow, dense outflow bounded on the polar side by a high-velocity stream, with most of the mass-loss from the fast stream as in the pure-radiative models (Proga et al. 2000). For stronger magnetic fields, first the slow part of the flow becomes denser and faster, and finally, the dense part of the wind dominates the mass-loss.

5. CONCLUSIONS AND FUTURE DIRECTIONS

Intrinsic absorption provides a "core sample" of an active nucleus and its host galaxy, thereby serving as a probe of the kinematics, physical conditions, geometry, and abundances in these regions. Because the gas is directly in the line of sight to the continuum source, the blueshifted absorption provides unambiguous evidence of outflow, whereas the kinematics of the BELR, for example, are still uncertain (Peterson 2003). In many cases, both radial and transverse velocities can be obtained for the absorbers, so they can be used as tracers of the dynamical forces (e.g., thermal winds, radiation pressure, magnetic forces, gravity) at work in AGN. The absorption features also provide a straightforward determination of the ionization state and hydrogen column density of the gas in the line of sight via photoionization models of the measured ionic column densities. Additional

constraints on the physical conditions (density, presence of dust) and geometry (global and line-of-sight covering factors, radial distances) can be obtained by a variety of means. Further constraints on the geometry are likely to come from observations of AGN at different orientations with respect to the line of sight because there are observational and theoretical indications that the properties of the absorbers (e.g., velocities, densities, columns) depend not only on their radial locations, but also on their polar angles with respect to the accretion disk axis. However, the properties of mass outflow almost certainly depend on other parameters as well, such as luminosity, black hole mass, accretion rate, and orientation of the active nucleus with respect to the host galaxy, and furthermore may actually evolve with time (Weymann 2002). Disentangling these effects will be a challenge, but will lead to a better understanding of each effect and its role in establishing the structure and dynamics of AGN.

Intrinsic absorption also yields clues to the relationship between AGN and their host galaxies. The absorption lines provide reliable abundances, which can be used to probe the star formation history of the nucleus and trace the chemical evolution of the inner regions of galaxies by observing quasars out to high redshifts (Hamann & Ferland 1999). Conversely, mass outflow deposits a significant amount of matter, momentum, and kinetic energy into the ISM, which may have a long-term impact on the dynamics of the ISM and star formation in the inner regions of the host galaxy (Weymann 2002).

Significant progress has been made in the determination of observational constraints on the absorbers and the development of sophisticated dynamical models. However, the study of intrinsic absorption is still in its infancy, and a detailed comparison between the observations and models has just begun. A "wish list" for future obervations includes intensive multiwavelength monitoring of a number of sources; to isolate the sources of variability; pin down the densities, locations, mass-loss rates, and other important parameters; and further determine the connection between the UV and X-ray absorbers. Higher S/N from future missions in the UV (e.g., the Cosmic Origins Spectrograph on HST) are crucial for determining the covering factors and degree of saturation of the absorption lines. Higher S/N and spectral resolution are needed in the X-ray (e.g., from the X-ray Spectrometer on Astro-E2 and the planned Constellation-X and X-ray Evolving Universe Spectroscopy (XEUS) missions) to resolve and measure the kinematic components of X-ray absorption. Clearly, observations of larger and more varied samples of objects are needed to explore the dependence of absorption properties on luminosity, AGN type, orientation, etc. For photoionization models of the X-ray absorbers, improvements in the basic atomic data for inner-shell transitions of many ions are needed. Fortunately, there are growing efforts to compare theoretical calculations with laboratory measurements and to prioritize the atomic data most urgently required from an astrophysical perspective (e.g., Behar & Kahn 2002). Most of the dynamical models have concentrated on BAL quasars and need fine-tuning to address the intrinsic UV and X-ray absorbers in Seyfert galaxies and quasars. Future efforts on hybrid models are likely to be fruitful

because it is almost certain that thermal winds, radiation pressure, magnetic fields, and gravity all play important roles in controlling the motions of the intrinsic absorbers.

ACKNOWLEDGMENTS

We thank all of our colleagues who supplied suggestions and comments during the preparation of this article. We extend special thanks to N. Arav, M. Bottorff, F. Bruhweiler, M. de Kool, J. Gabel, J. Kaastra, S. Kaspi, N. Murray, K. Nandra, D. Proga, and P. Wiita for help and careful reading of various parts of the manuscript. This work was supported by various grants from NASA. In addition, the authors acknowledge support from Georgia State University (DMC); The Catholic University of America (SBK); the University of Maryland, Baltimore County (IMG); and NASA's Goddard Space Flight Center (SBK and IMG).

The *Annual Review of Astronomy and Astrophysics* is online at http://astro.annualreviews.org

LITERATURE CITED

Abbott DC. 1982. *Ap. J.* 259:282–301

Ali B, Blum RD, Bumgardner TE, Cranmer SR, Ferland GJ, et al. 1991. *PASP.* 103:1182–86

Anderson KS, Kraft RP. 1969. *Ap. J.* 158: 859–64

Antonucci R. 1993. *Annu. Rev. Astron. Astrophys.* 31:473–521

Arav N. 1997. See Arav et al. 1997, 128:208–13

Arav N, Becker RH, Laurent-Muehleisen SA, Gregg MD, White RL, et al. 1999. *Ap. J.* 524:566–71

Arav N, Korista KT, de Kool M. 2002b. *Ap. J.* 566:699–704

Arav N, Li Z-Y. 1994. *Ap. J.* 427:700–7

Arav N, Li Z-Y, Begelman MC. 1994. *Ap. J.* 432:62–74

Arav N, Shlosman I, Weymann RJ, eds. 1997. *Mass Ejection from Active Galactic Nuclei*, ASP Conf. Ser. 128. San Francisco: Astron. Soc. Pac.

Arnaud KA, Branduardi-Raymont G, Culhane JL, Fabian AC, Hazard C, et al. 1985. *MNRAS.* 217:105–13

Baker JC, Hunstead RW, Athreya RM, Barthel PD, de Silva, E, et al. 2002. *Ap. J.* 568:592–609

Baldwin JA, Ferland GJ, Korista KT, Hamann F, Dietrich M. *Ap. J.* 582:590–95

Balsara DS, Krolik JH. 1993. *Ap. J.* 402:109–24

Barenblatt GI, Zel'Dovich YaB. 1972. *Annu. Rev. Fluid Mech.* 4:285–312

Barvainis R. 1987. *Ap. J.* 320:537–44

Begelman MC, McKee CF, Shields GA. 1983. *Ap. J.* 271:70–88

Behar E, Kahn S. 2002. *High energy astrophysics—X-ray spectroscopy and atomic data*. Presented at NASA Lab. Astrophys. Worksh., NASA-Ames Res. Cent., Moffet Field, CA, May 1–3

Blandford RD, Payne DG. 1982. *MNRAS.* 199:883–903

Blustin AJ, Branduardi-Raymont G, Behar E, Kaastra JS, Kahn SM, et al. 2002. *Astron. Astrophys.* 392:453–67

Boksenberg A, Snijders MAJ, Wilson R, Benvenuti P, Clavel J, et al. 1978. *Nature* 275:404–14

Boller Th, Brandt WN, Fink H. 1996. *Astron. Astrophys.* 305:53–73

Boller Th, Fabian AC, Sunyaev S, Trümper J, Fabian AC, et al. 2002. *MNRAS.* 329: L1–5

Bottorff MC, Korista KT, Shlosman I. 2000. *Ap. J.* 537:134–51

Bottorff MC, Korista KT, Shlosman I, Blandford RD. 1997. *Ap. J.* 479:200–21

Bradt HVD, Ohashi T, Pounds KA. 1992. *Annu. Rev. Astron. Astrophys.* 30:391–427

Brandt WN, Heap SR, Beaver EA, Boggess A, Carpenter KG, et al. 1994. *PASP.* 106:890–908

Brandt WN, Fabian AC, Pounds KA. 1996. *MNRAS.* 278:326–36

Brandt WN, Laor A, Wills BJ. 2000. *Ap. J.* 528:637–49

Brinkman AC, Gunsing CJ, Kaastra JS, Braeuninger HW, Hartner GD, et al. 1997. *Proc. SPIE* 3113:181–92

Bromage GE, Boksenberg A, Clavel J, Elvius A, Penston MV, et al. 1985. *MNRAS.* 215:1–36

Brotherton MS, Green RF, Kriss GA, Oegerle W, Kaiser ME, et al. 2002. *Ap. J.* 565:800–7

Burke BE, Mountain RW, Daniels PJ, Cooper MT, Dolat VS. 1993. *Proc. SPIE* 2006:272–85

Castor JI, Abbott DC, Klein RI. 1975. *Ap. J.* 195:157–74

Chandrasekhar S. 1945. *Ap. J.* 124:232–43

Chelouche D, Netzer H. 2001. *MNRAS.* 326:916–26

Clavel J, Reichert GA, Alloin D, Crenshaw DM, Kriss G, et al. 1991. *Ap. J.* 366:64–81

Collinge MJ, Brandt WN, Kaspi S, Crenshaw DM, Elvis M, et al. 2001. *Ap. J.* 557:2–17

Crenshaw DM, Boggess A, Wu C. 1995. *Astron. J.* 110:1026–31

Crenshaw DM, Kraemer SB. 1999. *Ap. J.* 521: 572–76

Crenshaw DM, Kraemer SB. 2001. *Ap. J.* 562: L29–33

Crenshaw DM, Kraemer SB, Boggess A, Maran SP, Mushotzky RF, Wu C. 1999. *Ap. J.* 516:750–768 (C99)

Crenshaw DM, Kraemer SB, Bruhweiler FC, Ruiz JR. 2001. *Ap. J.* 555:633–40

Crenshaw DM, Kraemer SB, Gabel JR, Kaastra JS, Steenbrugge KC, et al. 2003. *Ap. J.* In press

Crenshaw DM, Kraemer SB, George IM, eds. 2002a. *Mass Outflow in Active Galactic Nuclei: New Perspectives. Astron. Soc. Pac. Conf. Ser. 255*. San Francisco: Astron. Soc. Pac. 435 pp.

Crenshaw DM, Kraemer SB, Hutchings JB, Bradley LD, Gull TR, et al. 2000a. *Astron. J.* 120:1731–38

Crenshaw DM, Kraemer SB, Hutchings JB, Danks AC, Gull TR, et al. 2000b. *Ap. J.* 545:L27–30

Crenshaw DM, Kraemer SB, Turner TJ, Collier S, Peterson BM, et al. 2002b. *Ap. J.* 566:187–94

Davidsen AF, Hartig GF. 1978. Presented at *COSPAR, Plenary Meet.*, 21st, May 29–June 10, Innsbruck, Austria

de Kool M, Arav N, Becker RH, Gregg MD, White R. 2001. *Ap. J.* 548:609–23

de Kool M, Begelman MC. 1995. *Ap. J.* 455:448–55

den Herder JW, Brinkman AC, Kahn SM, Branduardi-Raymont G, Thomsen K, et al. 2001. *Astron. Astrophys.* 365:L7–17

Elvis M. 2000. *Ap. J.* 545:63–76

Emmering RT, Blandford RD, Shlosman I. 1992. *Ap. J.* 385:460–77

Espey BR, Kriss GA, Krolik JH, Zheng W, Tsvetanov Z, Davidsen AF. 1998. *Ap. J.* 500:L13–16

Evans IN, Ford HC, Kinney AL, Antonucci RRJ, Armus L, Caganoff S. 1991. *Ap. J.* 369:L27–30

Fabian AC, Kunieda H, Inoue S, Matsuoka M, Mihara T, et al. 1994. *PASJ.* 46:L59–63

Ferland GJ, Korista KT, Verner DA, Ferguson JW, Kingdon JB, Verner EM. 1998. *PASP.* 110:761–78

Filippenko AV, Ho LC, Sargent WLW. 1993. *Ap. J.* 410:L75–78

Fiore F, Elvis M, Mathur S, Wilkes BJ, McDowell JC. 1993. *Ap. J.* 415:129–39

Foltz CB, Weymann RJ, Peterson BM, Sun L, Malkan MA, Chaffee FH. 1986. *Ap. J.* 307:504–34

Gabel JR, Crenshaw DM, Kraemer SB, Brandt WN, George IM, et al. 2003. *Ap. J.* 583: 178–91

Gallagher SC, Brandt WN, Chartas G, Garmire GP. 2002. *Ap. J.* 567:37–41

Gallimore JF, Baum SA, O'Dea CP, Brinks E, Pedlar A. 1996. *Ap. J.* 462:740–45

Ganguly R, Bond NA, Charlton JC, Eracleous M, Brandt WN, Churchill CW. 2001. *Ap. J.* 549:133–54

Ganguly R, Eracleous M, Charlton JC, Churchill CW. 1999. *Astron. J.* 117:2594–607

George IM, Fabian AC. 1991. *MNRAS.* 249: 352–67

George IM, Mushotzky RF, Turner TJ, Yaqoob T, Ptak A, et al. 1998a. *Ap. J.* 509:146–62

George IM, Turner TJ, Mushotzky RF, Nandra K, Netzer H. 1998b. *Ap. J.* 503:174–85

George IM, Turner TJ, Netzer H, Nandra K, Mushotzky RF, Yaqoob T. 1998c. *Ap. J. Suppl.* 114:73–120

George IM, Turner TJ, Yaqoob T, Netzer H, Laor A, et al. 2000. *Ap. J.* 531:52–80

Gondoin P, Barr P, Lumb D, Oosterbroek T, Orr A, Parmar AN. 2001a. *Astron. Astrophys.* 378:806–16

Gondoin P, Lumb D, Siddiqui H, Guainazzi M, Schartel N. 2001b. *Astron. Astrophys.* 373:805–15

Gondoin P, Orr A, Lumb D, Santos-Lleo M. 2002. *Astron. Astrophys.* 388:74–87

Goodrich RW, Miller JS. 1995. *Ap. J.* 448:L73–76

Green PJ, Schartel N, Anderson SF, Hewett PC, Foltz CB, et al. 1995. *Ap. J.* 450:51–63

Green PJ, Aldcroft TL, Mathur S, Wilkes BJ, Elvis M. 2001. *Ap. J.* 558:109–18

Green PJ, Aldcroft TL, Mathur S, Wilkes BJ, Elvis M. 2002. See Crenshaw et al. 2002a, 255:19–24

Greenhill LJ, Gwinn CR, Antonucci R, Barvainis R. 1996. *Ap. J.* 472:L21–24

Grevesse N, Anders E. 1989. In *Cosmic Abundances of Matter*, ed. CJ Waddington, AIP Conf. Proc. 183:1–8. New York: AIP

Guainazzi M, Matsuoka M, Piro L, Mihara T, Yamauchi M. 1994. *Ap. J.* 436:L35–39

Halpern JP. 1984. *Ap. J.* 281:90–94

Hamann F, Barlow TA, Chaffee FC, Foltz CB, Weymann RJ. 2001. *Ap. J.* 550:142–52

Hamann F, Barlow TA, Cohen RD, Junkkarinen V, Burbidge EM. 1997a. See Arav et al. 1997, 128:19–24

Hamann F, Barlow TA, Junkkarinen V. 1997b. *Ap. J.* 478:87–93

Hamann F, Barlow TA, Junkkarinen V, Burbidge EM. 1997c. *Ap. J.* 478:80–86

Hamann F, Ferland G. 1999. *Annu. Rev. Astron. Astrophys.* 37:487–531

Harms R, Fitch J. 1991. *Proc. SPIE* 1494:49–65

Iwasawa K, Fabian AC, Almaini O, Lira P, Lawrence A, et al. 2000. *MNRAS.* 318:879–88

Jansen F, Lumb D, Alteri B, Clavel J, Ehle M, et al. 2001. *Astron. Astrophys.* 365:L1–6

Kaastra JS, Steenbrugge KC, Raassen AJJ, van der Meer RLJ, Brinkman AC, et al. 2002. *Astron. Astrophys.* 386:427–45

Kallman T, Bautista M. 2001. *Ap. J. Suppl.* 133: 221–53

Kaspi S, Brandt WN, George IM, Netzer H, Crenshaw DM, et al. 2002. *Ap. J.* 574:643–62

Kaspi S, Brandt WN, Netzer H, George IM, Chartas G, et al. 2001. *Ap. J.* 554:216–232

Kaspi S, Brandt WN, Netzer H, Sambruna R, Chartas G, et al. 2000. *Ap. J.* 535:L17–20

Khachikian EY, Weedman DW. 1971. *Astrofizika* 7:389–406

Kimble RA, Woodgate BE, Bowers CW, Kraemer SB, Kaiser ME, et al. 1998. *Ap. J.* 492:L83–93

Komossa S, Bade N. 1998. *Astron. Astrophys.* 331:L49–52

Komossa S. 1999. In *Japan-Germany Workshop on AGN and the X-ray Background*, eds. T Takahashi, H Inoue, ISAS Rep., pp. 149–60. Tokyo: Inst. Space Astron. Sci.

Königl A, Kartje J. 1994. *Ap. J.* 424:446–67

Korista KT, Alloin D, Barr P, Clavel J, Cohen RD, et al. 1995. *Ap. J. Suppl.* 97:285–330

Kraemer SB, Crenshaw DM, Gabel JR. 2001a. *Ap. J.* 557:30–38

Kraemer SB, Crenshaw DM, George IM, Netzer H, Turner TJ, Gabel JR. 2002. *Ap. J.* 577:98–113

Kraemer SB, Crenshaw DM, Hutchings JB,

George IM, Danks AC, et al. 2001b. *Ap. J.* 551:671–86
Kraemer SB, Crenshaw DM, Hutchings JB, Gull TR, Kaiser ME, et al. 2000a. *Ap. J.* 531:278–95
Kraemer SB, Crenshaw DM, Yaqoob T, McKernan B, Gabel JR, et al. 2003. *Ap. J.* 582:125–32
Kraemer SB, George IM, Turner TJ, Crenshaw DM. 2000b. *Ap. J.* 535:53–57
Kraemer SB, Ho LC, Crenshaw DM, Shields JC, Filippenko AV. 1999. *Ap. J.* 520:564–73
Kriss GA. 1997. In *Emission Lines in Active Galaxies: New Methods and Techniques*, eds. BM Peterson, F-Z Cheng, AS Wilson, ASP Conf. Ser. 113:453–56. San Francisco: Astron. Soc. Pac.
Kriss GA. 2002. See Crenshaw et al. 2002a, 255:69–74
Kriss GA, Davidsen AF, Blair WP, Bowers CW, Dixon WV, et al. 1992. *Ap. J.* 392:485–491
Kriss GA, Davidsen AF, Zheng W, Kruk JW, Espey BR. 1995. *Ap. J.* 454:L7–10
Kriss GA, Espey BR, Krolik JH, Tsvetanov Z, Zheng W, Davidsen AF. 1996a. *Ap. J.* 467:622–28
Kriss GA, Green RF, Brotherton M, Oegerle W, Sembach KR, et al. 2000. *Ap. J.* 538:L17–21
Kriss GA, Krolik JH, Otani C, Espey BR, Turner TJ, et al. 1996b. *Ap. J.* 467:629–35
Krolik JH, Begelman MC. 1986. *Ap. J.* 308: L55–58
Krolik JH, Begelman MC. 1988. *Ap. J.* 329: 702–11
Krolik JH, Kriss GA. 1995. *Ap. J.* 447:512–25
Krolik JH, Kriss GA. 1997. See Arav et al. 1997, 128:132–38
Krolik JH, Kriss GA. 2001. *Ap. J.* 561:684–90
Krolik JH, McKee CF, Tarter CB. 1981. *Ap. J.* 249:422–42
Kruk JW, Durrance ST, Kriss GA, Davidsen AF, Blair WP, et al. 1995. *Ap. J.* 454:L1–6
Laor A, Brandt WN. 2002. *Ap. J.* 569:641–54
Laor A, Draine BT. 1993. *Ap. J.* 402:441–68
Laor A, Fiore F, Elvis M, Wilkes BJ, McDowell JC. 1997. *Ap. J.* 477:93–113
Lawrence A, Elvis M. 1982. *Ap. J.* 256:410–26
Lee JC, Ogle PM, Canizares CR, Marshall HL, Schultz NS, et al. 2001. *Ap. J.* 554:L13–17
Maeder A, Maynet G. 1989. *Astron. Astrophys.* 210:155–73
Maran SP, Crenshaw DM, Mushotzky RF, Reichert GA, Carpenter KG, et al. 1996. *Ap. J.* 465:733–37
Markert TH, Canizares CR, Dewey D, McGuirk M, Pak CS, Schattenburg ML. 1994. *Proc. SPIE* 2280:168–80
Marshall HL, Edelson RA, Vaughan S, Malkan MA, O'Brien P, Warwick RS. 2003. *Astron. J* 125:459–64
Mason KO, Branduardi-Raymont G, Ogle PM, Page MJ, Puchnarewicz EM, et al. 2003. *Ap. J.* 582:95–104
Mathews WG, Ferland GJ. 1987. *Ap. J.* 323:456–67
Mathis JS, Rumpl W, Nordsieck KH. 1977. *Ap. J.* 217:425–33
Mathur S. 1994. *Ap. J.* 431:L75–78
Mathur S, Elvis M, Wilkes B. 1995. *Ap. J.* 452:230–37
Mathur S, Wilkes BJ, Aldcroft T. 1997. *Ap. J.* 478:182–89
Mathur S, Wilkes B, Elvis M, Fiore F. 1994. *Ap. J.* 434:493–502
Matsuoka M, Piro L, Yamauchi M, Murakami T. 1990. *Ap. J.* 361:440–58
Mestel L. 1961. *MNRAS.* 122:473–78
Mihara T, Matsuoka M, Mushotzky RF, Kuniedo H, Otani C, et al. 1994. *PASJ.* 46:L137–40
Miller JS, Antonucci RRJ. 1983. *Ap. J.* 271:L7–11
Mineo T, Stewart GC. 1993. *MNRAS.* 262:817–22
Moos HW, Cash WC, Cowie LL, Davidsen AF, Dupree AK, et al. 2000. *Ap. J.* 538:L1–6
Moran EC, Filippenko AV, Ho LC, Shields JC, Belloni T, et al. 1999. *PASP.* 111:801–8
Morales R, Fabian AC, Reynolds CS. 2000. *MNRAS.* 315:149–54
Morton DC. 1991. *Ap. J. Suppl.* 77:119–202
Morton DC, York DG, Jenkins EB. 1988. *Ap. J. Suppl.* 68:449–61
Murray N, Chiang J. 1995. *Ap. J.* 454:L105–9

Murray N, Chiang J, Grossman SA, Voit GM. 1995. *Ap. J.* 451:498–509

Mushotzky RF, Done C, Pounds KA. 1993. *Annu. Rev. Astron. Astrophys.* 31:717–61

Nandra K, Fabian AC, George IM, Branduardi-Raymont G, Lawrence A, et al. 1993. *MNRAS.* 260:504–12

Nandra K, George IM, Mushotzky RF, Turner TJ, Yaqoob T. 1997. *Ap. J.* 477: 602–22

Nandra K, Pounds KA. 1992. *Nature* 359:215–16

Nandra K, Pounds KA. 1994. *MNRAS.* 268:405–29

Nandra K, Pounds KA, Stewart GC. 1990. *MNRAS.* 242:660–68

Netzer H. 1990. *Active Galactic Nuclei*, ed. T Courvoisier, M Mayor. Berlin: Springer

Netzer H. 1993. *Ap. J.* 411:594–601

Netzer H. 1996. *Ap. J.* 473:781–96

Netzer H, Chelouche D, George IM, Turner TJ, Crenshaw DM, et al. 2002. *Ap. J.* 571:256–64

Nicastro F, Fiore F, Matt G. 1999a. *Ap. J.* 517:108–22

Nicastro F, Fiore F, Perola G, Elvis M. 1999b. *Ap. J.* 514:184–96

O'Brien PT, Page K, Reeves JN, Pounds KA, Turner MJL, Puchnarewicz EM. 2001. *MNRAS.* 327:L37–41

Ogle PM, Marshall HL, Lee JC, Canizares CR. 2000. *Ap. J.* 545:L81–84

Oke JB, Sargent WLW. 1968. *Ap. J.* 151:807–24

Osterbrock DE. 1989. *Astrophysics of Gaseous Nebulae and Active Galactic Nuclei*. Mill Valley, CA: Univ. Sci. Books. 408 pp.

Otani C, Kii K, Reynolds CS, Fabian AC, Iwasawa K. et al. 1996. *PASJ.* 48:211–18

Pan HC, Stewart GC, Pounds KA. 1990. *MNRAS.* 242:177–87

Penston MV, Boksenberg A, Bromage GE, Clavel J, Elvius A, et al. 1981. *MNRAS.* 196:857–87

Peterson BM. 1997. *An Introduction to Active Galactic Nuclei*. Cambridge, UK: Cambridge Univ. Press. 238 pp.

Peterson BM. 2003. *Hubble's Science Legacy: Future Optical-Ultraviolet Astronomy from Space*, eds. KR Sembach, JC Blades, CD Illingworth, RC Kennicutt, ASP Conf. Ser. 291. In press. San Francisco: Astron. Soc. Pac.

Peterson BM, Wandel A. 2000. *Ap. J.* 540:L13–16

Phinney ES. 1989. In *Theory of Accretion Disks, Proceedings of a NATO Advanced Research Workshop*, ed. F Meyer, NATO ASI Series C, Vol. 290:457. Dordrecht: Kluwer

Pier EA, Krolik JH. 1992. *Ap. J.* 399:L23–26

Pogge RW, de Robertis MM. 1993. *Ap. J.* 404:563–69

Porquet D, Dubau J. 2000. *Astron. Astrophys. Suppl.* 143:495–514

Pounds KA, Nandra K, Fink HH, Makino F. 1994. *MNRAS.* 267:193–208

Pounds KA, Nandra K, Stewart GC, George IM, Fabian AC. 1990. *Nature* 344:132–33

Pounds KA, Nandra K, Stewart GC, Leighly K. 1989. *MNRAS.* 240:769–83

Pounds K, Reeves J, O'Brien P, Page K, Turner M, Nayakshin S. 2001. *Ap. J.* 559:181–86

Proga D. 2003. *Ap. J.* 585:406–17

Proga D, Stone JM, Kallman TR. 2000. *Ap. J.* 543:686–96

Ptak A, Yaqoob T, Serlemitsos PJ, Mushotzky RF, Otani C. 1994. *Ap. J.* 435:L31–34

Rees MJ. 1987. *MNRAS.* 228:47P–50

Rees MJ, Netzer H, Ferland GJ. 1989. *Ap. J.* 347:640–655

Reeves JN, Turner MJL. 2000. *MNRAS.* 316:234–48

Reynolds CS. 1997. *MNRAS.* 286:513–37

Reynolds CS, Fabian AC, Nandra K, Inoue H, Kunieda H, Iwasawa K. 1995. *MNRAS.* 277:901–12

Risaliti G, Elvis M, Nicastro F. 2002. *Ap. J.* 571: 234–46

Romano P, Mathur S, Pogge RW, Peterson BM, Kuraszkiewicz J. 2002. *Ap. J.* 578:64–73

Ruiz JR, Crenshaw DM, Kraemer SB, Bower GA, Gull TR, et al. 2001. *Astron. J.* 122:2961–68

Safier PN. 1993a. *Ap. J.* 408:115–47

Safier PN. 1993b. *Ap. J.* 408:148–59

Sahnow DJ, Moos HW, Ake TB, Andersen J, Andersson B-G, et al. 2000. *Ap. J.* 538: L7–11

Sako M, Kahn SM, Behar E, Kaastra JS, Brinkman AC, et al. 2001. *Astron. Astrophys.* 365:L168-L173
Sako M, Kahn SM, Branduardi-Raymont G, Kaastra JS, Brinkman AC, et al. 2003. *Ap. J.* In press
Savage BD, Sembach KR. 1991. *Ap. J.* 379: 245–59
Scoville N, Norman C. 1995. *Ap. J.* 451:510–24
Seyfert CK. 1943. *Ap. J.* 97:28–40
Shakura NI, Sunyaev RA. 1973. *Astron. Astrophys.* 24:337–55
Shields JC, Hamann F. 1997. *Ap. J.* 481:752–57
Shields JC, Sabra BM, Ho LC, Barth AJ, Filippenko AV. 2002. See Crenshaw et al. 2002a, 255:105–9
Shull JM, van Steenberg ME. 1985. *Ap. J.* 294:599–614
Spitzer L. 1978. In *Physical Processes in the Interstellar Medium* New York: Wiley-Intersci. 333 pp
Sprayberry D, Foltz CB. 1992. *Ap. J.* 390:39–45
Tanaka Y, Inoue H, Holt SS. 1994. *PASJ* 46:L37–41
Turner TJ, George IM, Mushotzky RF. 1993a. *Ap. J.* 412:72–81
Turner TJ, George IM, Nandra K, Mushotzky RF. 1998. *Ap. J.* 493:91–101
Turner TJ, Nandra K, George IM, Fabian AC, Pounds KA. 1993b. *Ap. J.* 419:127–135
Turner TJ, Romano P, George IM, Edelson R, Collier SJ, et al. 2001. *Ap. J.* 561:131–45
Turner TJ, Romano P, Kraemer SB, George IM, Yaqoob T, et al. 2002. *Ap. J.* 568:120–32
Turner TJ, Weaver KA, Mushotzky RF, Holt SS, Madejski GM. 1991. *Ap. J.* 381:85–100
Ulrich MH. 1988. *MNRAS.* 230:121–30
Vestergaard M. 2003. *Ap. J.* In press
Verner DA, Ferland G, Korista KT, Yakovlev DG. 1996. *Ap. J.* 465:487–98
Verner DA, Yakovlev DG. 1995. *Astron. Astrophys. Suppl.* 109:125–33
Verner EM, Verner DA, Korista KT, Ferguson JW, Hamann F, Ferland GJ. 1999. *Ap. J. Suppl.* 120:101–12
Warwick RS, Pounds KA, Turner TJ. 1988. *MNRAS.* 231:1145–52
Weaver KA, Yaqoob T, Holt SS, Mushotzky RF, Matsuoka M, Yamauchi M. 1994. *PASJ.* 436:L27–30
Weisskopf MC, O'dell SL, van Speybroeck LP. 1996. *Proc. SPIE* 2805:2–7
Weymann RJ. 2002. See Crenshaw et al. 2002a, 255:329–39
Weymann RJ, Carswell RF, Smith MG. 1981. *Annu. Rev. Astron. Astrophys.* 19:41–76
Weymann RJ, Morris SL, Gray ME, Hutchings JB. 1997. *Ap. J.* 483:717–30
Wilson AS, Braatz JA, Heckman TM, Krolik JH, Miley GK. 1993. *Ap. J.* 419:L61–64
Woodgate BE, Kimble RA, Bowers CW, Kraemer S, Kaiser ME, et al. 1998. *PASP.* 110:1183–204
Yaqoob T, McKernan B, Kraemer SB, Crenshaw DM, Gabel JR, et al. 2003. *Ap. J.* 582:105–24
Yaqoob TJ, Serlemitsos PJ, Mushotzky RF, Madejski GM, Turner TJ, Kuniedo H. 1994. *PASJ.* 46:L173–77
Yaqoob T, Warwick RS, Pounds KA. 1989. *MNRAS.* 236:153–70
Zheng W, Kriss GA, Telfer RC, Grimes JP, Davidsen AF. 1997. *Ap. J.* 475:469–78

Annual Review of Astronomy and Astrophysics
Volume 41, 2003

CONTENTS